POLYPEPTIDE BASED NANOPARTICLES FOR PHOTOTHERMAL THERAPY OF CANCER

M.Sc. Thesis

By

KALPANA KUMARI

DISCIPLINE OF BIOSCIENCES AND BIOMEDICAL ENGINEERING

INDIAN INSTITUTE OF TECHNOLOGY INDORE

JUNE 2019

POLYPEPTIDE BASED NANOPARTICLES FOR PHOTOTHERMAL THERAPY OF CANCER

A THESIS

Submitted in partial fulfillment of the requirements for the award of the degree

of

Master of Science

by

KALPANA KUMARI

DISCIPLINE OF BIOSCIENCES AND BIOMEDICAL ENGINEERING

INDIAN INSTITUTE OF TECHNOLOGY INDORE

JUNE 2019

INDIAN INSTITUTE OF TECHNOLOGY INDORE

CANDIDATE'S DECLARATION

I hereby certify that the work which is being presented in the thesis entitled **POLYPEPTIDE BASED NANOPARTICLES FOR PHOTOTHERMAL THERAPY OF CANCER** in thepartial fulfillment of the requirements for the award of the degree of **MASTER OF SCIENCE** and submitted in the **DISCIPLINE OF BIOSCIENCES AND BIOMEDICAL ENGINEERING, Indian Institute of Technology Indore**, is an authentic record of my own work carried out during the time period from May, 2018 to June, 2019 under the supervision of Dr. Sharad Gupta, Assistant Professor.

The matter presented in this thesis has not been submitted by me for the award of any other degree of this or any other institgnature of the student with date

(KALPANA KUMARI)

This is to certify that the above statement made by the candidate is correct to the best of my knowledge.

Signature of the Supervisor with date
(DR. SHARAD GUPTA)

KALPANA KUMARIhas successfully given her M.Sc. Oral Examination held on **26 JUNE 2019.**

SignatureofSupervisorof MSc thesis
Date:

Convener, DPGC
Date:

Signature of PSPC Member #1

Signature of PSPC Member #2

ACKNOWLEDGEMENTS

Starting with the first two persons of my life,I would deeply express my love and gratitude towards my lovable mother, father, and family members for their continuoussupport throughout this journey.

I want to express my sincere gratitude to **Dr. Sharad Gupta,** my supervisor, for providing the opportunity to work in his lab. I am highly grateful to him for his continuous support and guidance throughout the study.

Iwould like to express my deep sense of indebtedness to **Ms. Anshu Kumari** (Ph.D. scholar) for giving me a foundation in the research field. I greatly acknowledge her support and encouragement to accomplish this work in spite of her extremely busy schedule. I am thankful to her for constant encouragement throughout the research work.

Further,I am thankful to my PSPC committee **Dr. Debasis Nayak** and **Dr. Chelvam Venkatesh**, head of the discipline **Dr. Hem Chandra Jha**, our project coordinator **Dr. Parimal Kar,** and DPGC convener **Dr. Kiran Bala** for their support and valuable advice regarding research.

I would like to thank **Dr. I. A. Palani,** for his kind help in the laser experiment and his student **Mr. M. Manikandan** for his patient and valuable time without which it was impossible to do the experiment.

This work is carried out at the Indian Institute of Technology Indore. I, duly acknowledge the infrastructure and research facility provided by the department, Discipline of Biosciences and Biomedical Engineering (**BSBE**) and Sophisticated Instrument Center (**SIC**).

I am thankful to Dr. Gupta and Dr. Nayak lab members Ms. Saumya Jaiswal, Mr. Surjendu Bikas Dutta, Mr. Prashant Kharey, Mr. Anurag Ramsuman Mishra, Mr. Ritudhuwaj Tiwary, Mrs. Prativa Majee, Mrs. Shruti Pyasi, Mr. Venkata Narayana Are, Mr. Basant Pravas Sahu and especially **Mrs. Suman Bishnoi** for their help and support.

I would like to extend my sincere thank to Amit Mishra, Arif Patel, and Murphy Bhaskar Ganveer for their help regarding instrumentation and administrative support.

I would also like to thank academic authorities, library authorities of IIT Indore, other technical and non-technical staffs for their constant support whenever required.

This acknowledgment is incomplete without expressing the special thanks to Bhanu Priya for always being there in my difficult situations.

I would like to express my sincere thanks and gratitude towards my senior Mr. Mrinal Kashyap, for his constant help and support whenever required.

I would like to express my sincere thanks to my sister Kumari Khushbu for immeasurable support with the deepest sense of love and my ever-smiling friends, Neetu Rajak, Priyanka Yadav, Suchi Agrawal, Shubham Choudhary, Rahul Lamba, Sai K. Vehchalapu and Abhipsa Panda with whom this journey has been a joyful experience.

Kalpana Kumari

This thesis is dedicated to

My Beloved Family

&

My senior Anshu Kumari

Publication other than thesis

Anshu Kumari, **Kalpana Kumari,** and Sharad Gupta, "The effect of nanoencapsulation of ICG on two-photon bioimaging", RSC Advances, 2019, **9**, 18703 – 18712. (IF 3)

Abstract

Treatment of cancer is still a grand challenge due to the side-effects related to the currently available therapies. These include surgical intervention, radiation, and chemotherapy, which kill healthy cells along with the cancerous cells leading to several side effects such as hair loss, weight loss, etc. To overcome the limitations related to the techniques mentioned above, a new laser-based cancer therapy, i.e., photothermal therapy (PTT) has been adopted as an alternative due to its minimal side-effect. This technique requires laser light as a radiation source for treating cancer. In PTT, the radiation of laser results in the thermal ablation of the cancerous cells. However, it has been shown that the inclusion of the photosensitizers such as gold, platinum, benzoporphyrin derivative, a cyanine dye, *etc*.could increase the efficacy of PTT for cancer treatments. Currently, Indocyanine green (ICG), the only U.S. food and drug administration (FDA) approved exogenous chromophore, is being used for various clinical applications. In addition to other clinical applications, ICG also shows the photothermal effect and could be used as a sensitizer for PTT. However, the application of the ICG is limited due to its short circulation lifetime and poor optical stability. These limitations could be addressed by nanoencapsulation of the ICG within nanoparticles (NPs). In this study, we have encapsulated ICG within poly-L-lysine based nanoparticles for PTT. The synthesis of these nanoparticles was done by using a two-step self-assembly method. These nanoparticles were spherical with ~225 nm diameter. The encapsulated ICG showed high photostability and improved cellular uptake in comparison to free ICG. These NPs show significant photothermal effect than free ICG.

Keywords: ICG, PLL nanoparticles, photothermal therapy.

TABLE OF CONTENTS

LIST OF FIGURES

Chapter 5. Results and discussion

LIST OF TABLES

Chapter 1. Introduction

Chapter 2. Literature review

LIST OF ABBREVIATIONS

PLL	Poly-L-lysine
NPs	Nanoparticles
ICG	Indocyanine green
FDA	Food and drug administration
NIR	Near-infrared
PTT	Photothermal therapy
WHO	World health organization
NICPR	National Institute of Cancer Prevention and Research
EPR	Enhanced permeability and retention
PS	Photosensitizer
MS	Mesoporous silica
PEG	Polyethylene glycol
FA	Folic acid
DMEM	Dulbecco's modified Eagle medium
DMSO	Dimethyl sulphoxide
FBS	Fetal bovine serum
PBS	Phosphate buffered saline
A549	Human lung cancer cell line
HUH7	Human liver cancer cell line
HeLa	Human cervical cancer cell line
HEK	Human embryonic kidney cell line

DAPI	4,6-Diamidino-2-phenylindole
MTT	3-[4,5-Dimethylthiazole-2-yl]-2,5-diphenyltetrazolium bromide
NCCS	National Center for Cell Science
FE-SEM	Field-emission scanning electron microscopy
DLS	Dynamic light scattering
UV	Ultraviolet

Chapter 1

Introduction

1.1 Cancer statistics at a glance

Cancer is one of the most devastating diseases across the world[1]. According to the report of World Health Organization (WHO), 18.1 million new cancer patients have been registered annually, and 9.6 million deaths in 2018. It is the second most common cause of death in India after cardiovascular disease[2,3]. According to the report of the Indian council of medical research (ICMR) 2018, over 11,57,294 lakh newly cancer patients have been registered every year in India, and more than 7 lakh are dying[4]. As shown in Figure 1.1, the five most common types of cancer that are found in men are lung, oral cavity, stomach, colorectal, and oesophageal cancer[5,6]. On the otherhand, the five most common cancer in women are breast, cervical, colorectal, ovary, and stomach, their statistical analysis is shown in Figure1.2[7–9].

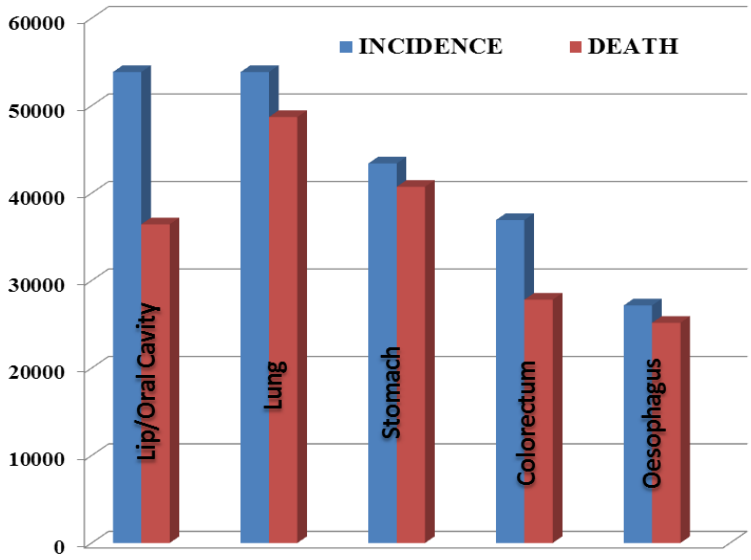

Figure 1.1 Five most common types of cancer found in men in India[8].

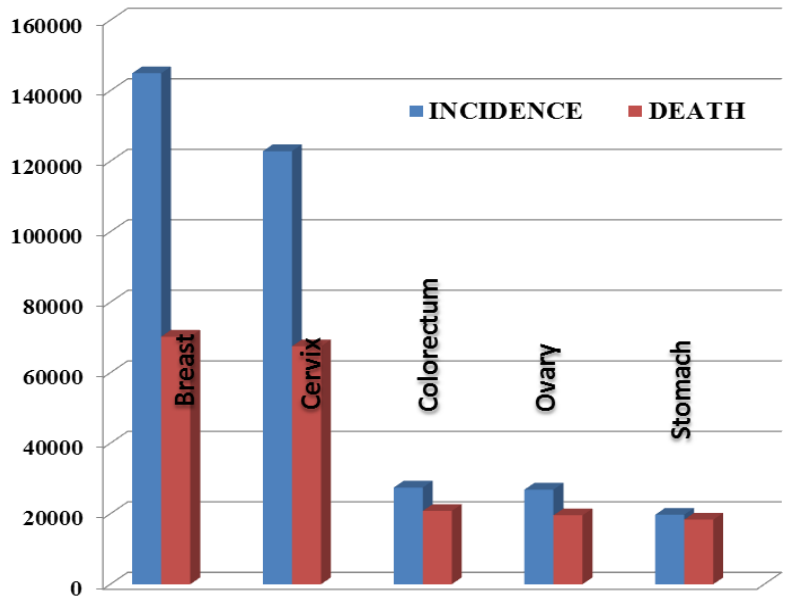

Figure 1.2 Five most common types of cancer found in women in India[9].

1.2 Cancer- Overview

Cancer is defined as the abnormal growth of cells where they lost the property of contact inhibition.These cells divide in an uncontrolled manner and form tumors. Tumors can be of two types- benign and malignant. A benign tumor does not invade nearby tissues, and it is non-cancerous, whereas malignant tumors can invade nearby tissues or distant part of the body through blood vessels or lymphatic system that form a secondary tumor. The metastatic property of the cancerous cell is one of the major challenges to completely cure cancer that causes more than 90% of death[10–12].

1.3 Causes of cancer

Various factors that cause cancer could majorly be classified into two categories: internal and external. Internal factors include inherent defects, gender, age, etc. The external factors include smoking, tobacco, exposure

to harmful radiations, alcohol consumption, lifestyle, virus, and other infections, etc.[13,14].

1.4 Conventional mode of cancer treatment

Cancer is generally treated by the conventional mode of treatment such as surgery, radiotherapy, chemotherapy[15], as shown in Figure 1.3.

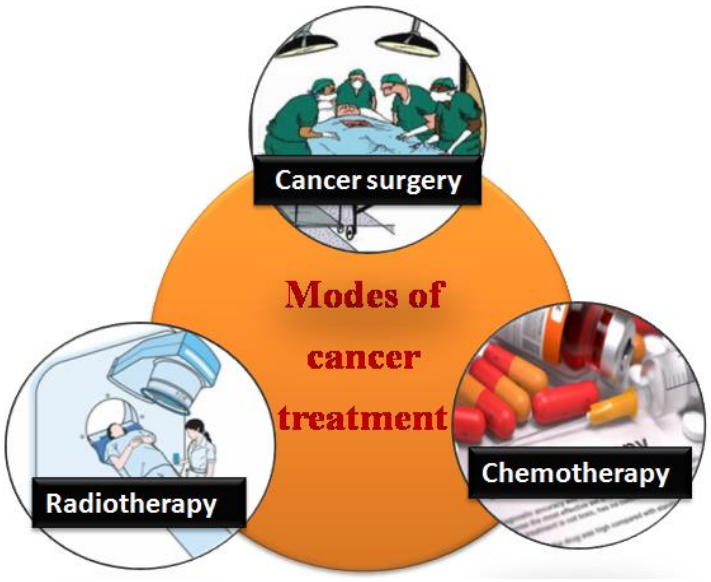

Figure 1.3 Three most common conventional mode of cancer treatment-cancer surgery, radiotherapy, and chemotherapy[15].

In cancer surgery, there is excision of cancer affected area. But sometimes, it may recur. That's why it is assisted by other modes of cancer treatments, i.e., radiotherapy and chemotherapy. In radiotherapy, harmful ionization radiations like gamma ray are being used to treat cancer. However, in chemotherapy, different varieties of chemotherapeutic drugs like doxorubicin are used to treat cancer. Cancer detection at an early stage is quite rare due to non-specific sign and symptoms, so, the success rate of cancer treatment at advanced stage and rate of survival of the patient is very less. Early diagnosis of cancer has a significant effect on the survival of cancer patient[16].

1.5 Limitations of the conventional mode of cancer treatment

Though the conventional mode of treatment can cure cancer, but it has several side-effects like lack of selectivity and specificity, systemic toxicity, multidrug resistance, high drug dosage requisite[17].To overcome these shortcomings, laser-based therapies could be an alternative approach for more efficient and specific in targeting the tumor tissue in comparison to the conventional mode of treatment.

1.6 Photothermal therapy- novel approach for cancer treatment

One of the laser-based approaches for the treatment of cancer is photothermal therapy (PTT) that emerged as a non-invasive localized therapeutic strategy to overcome the limitations of the conventional mode of treatment[40]. Photothermal therapy can be an alternative way for the tumor cell treatment through thermal ablation[41–44], and this therapy is localized invasive treatment that uses optical radiation in NIR or visible light range to convert this energy into heat. Photons are absorbed by the intracellular organelles as well as intercellular tissue, which elevates tissue temperature that results in tissue or cell death when a laser is irradiated on cancer tissues[45].

1.7 Nanocarriers an emerging platform for theranostics

The problem of non-specific delivery of the anti-cancer drugs can be addressed by encapsulating the drug or photosensitizers within nanocarriers. Nanoparticles come in several shapes like a rod, spherical, star, cubical, etc. owing to their origin and fabrication technique, they can either be natural or synthetic, as shown in Figure 1.4. These nanoparticles augment the half-life of the therapeutic agent of interest and can protect it from degradation. The nanoparticles can target the diseased tissue via active and passive targeting approach.

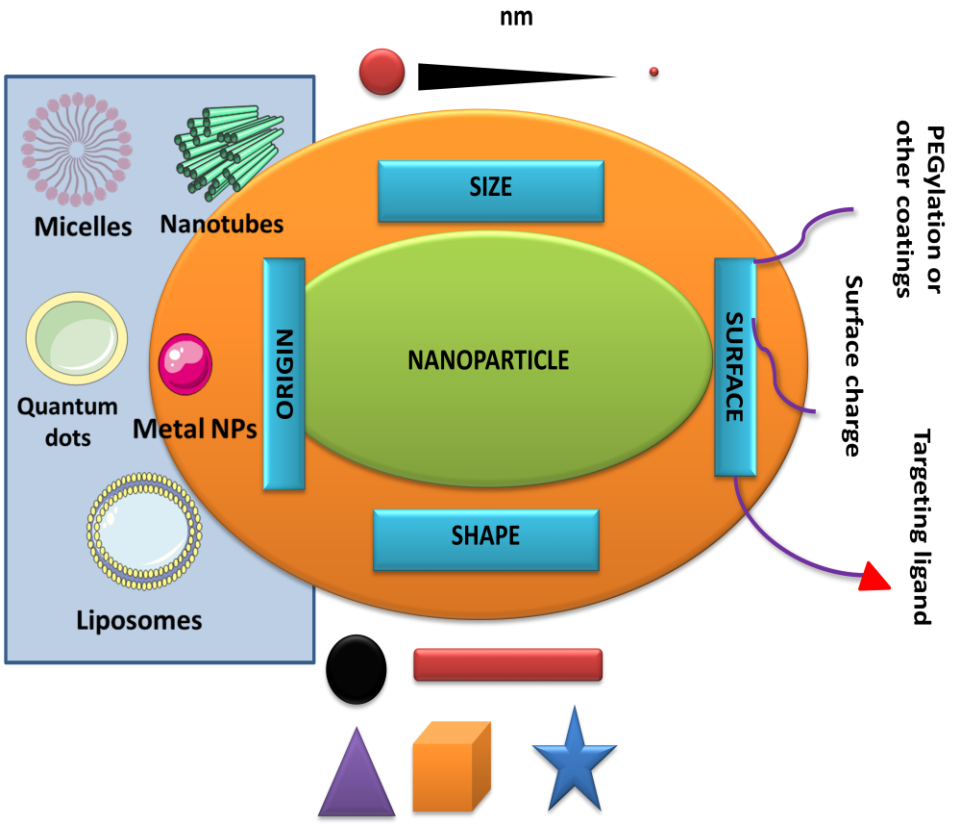

Figure1.4 Classification of nanoparticles on the based on their size, surface modification, shape, and fabrication material.

1.8 Tumor targeting via NP

1.8.1 Passive tumor targeting

An effective cancer drug should have a tendency to reach the tumor tissue. The tumor blood vessels have unique properties that include wide blood vessel formation[18], excessive blood vessel permeability[19], and lack of lymphatic drainage at the site of tumor tissues due to which NPs can use the property of leaky blood vessel so that easily able to enter and accumulate at the site of the cancer. This event is called the enhanced permeability and retention effect (EPR)[20,21] as shown in Figure 1.5. EPR effect makes the treatment of the solid tumor through passive targeting[22].

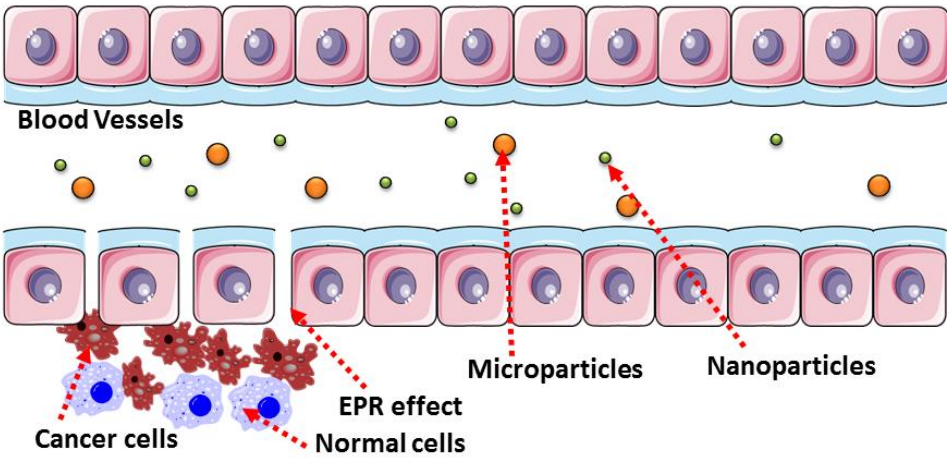

Figure 1.5 Mechanism of retention of nanoparticles onto the cancer site via enhanced permeability and retention effect[22].

1.8.2 Active tumor targeting

Enhanced permeability and retention effect vary from one type of cancer to others. Active tumor targeting is an effective way of delivering the drug-loaded nanoparticles. It is more specific in comparison to the passive tumor targeting since the targeting moieties are ligated on NP to make it more specific. Hence, it is a more effective therapeutic method[23].

Table 1. Different types of therapeutically active nanoparticles[24, 25, 34–39, 26–33].

Types of Nanoparticles	Structure	Characteristics
Polymeric nanoparticles	Drugs are conjugated to the side chain of a biodegradable linear polymer with a linker (cleavable bond)	a) Water-soluble, nontoxic, b) Surface modification c) Selective accumulation and retention in tumor tissue

Polymer micelles	Amphiphilic block copolymers assemble and form a micelle with a hydrophobic core and hydrophilic shell	a) Suitable carrier for water-insoluble drug b) Biocompatible, self-assembling, biodegradable c) Targeting potential d) Ease of functional modification
Dendrimers	The radially branched polymer structure	a) Biodistribution and pharmacokinetics can be tuned b) High structural and chemical homogeneity c) Ease of functionalization, high ligand density d) Control degradation e) Multifunctionality
Liposomes	Self-assembling closed colloidal structures	a) Amphiphilic, biocompatible b) Ease of modification
Viral nanoparticles	Protein cages which are multivalent self-assembled structures	a) Surface modification by mutagenesis or bioconjugation b) Specific tumor targeting multifunctionality
Carbon nanotubes	Carbon cylinders composed of the benzene ring	a) Water soluble and biocompatible through chemical modification b) Multifunctionality

There are varieties of nanoparticles that could be used for therapeutics, are listed in Table 1 along with their details[24, 25, 34–39, 26–33].

Chapter 2

Literature review

2.1 Background

There are various exogenous chromophores such as porphyrin, chlorin, bacteriochlorin, indocyanine green, etc. that are reported to use in the field oftheranostics[47-49,50] Among all the reported photosensitizers, Indocyanine green (ICG) is a food and drug administration (FDA) approved dye that is widely used in NIR optical window for theranostics[51–53]. The nearinfrared (NIR) window is widely used in the field of optical disease diagnosis and therapeutics[46]. This region is used because of low scattering, least absorption,and negligible autofluorescence in biological tissues[55,56].

2.2 Properties of ICG

ICG is a cyanine dye that consists of two sulphonate group and has a molecular weight of 774.96 Da[57]. The molecular structure of ICG is shown in Figure 2.1. The NIR optical absorbance and emission of ICG is lying in the range of 600 nm-900 nm[58].

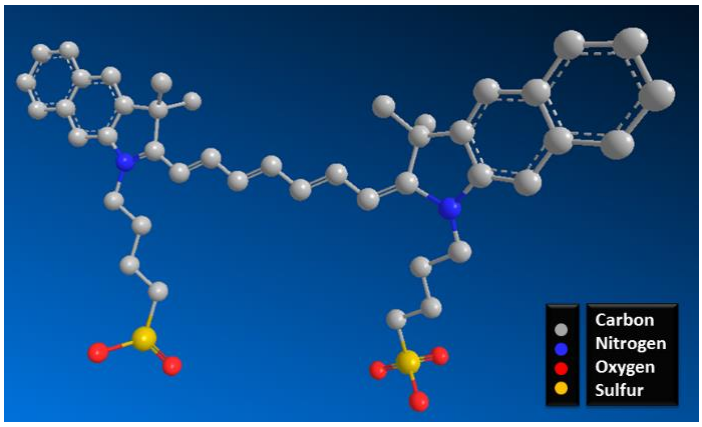

Figure 2.1 Molecular structure of the Indocyanine green.

Specifically, the absorption and emission maxima are around 780 nm and

810 nm, respectively[59]. It is a negatively charged and amphiphilic molecule[61]. It has a short half-life (2-4 minutes) in blood circulation due to non-specific binding with plasma[62, 63]. ICG can be used as photosensitizers in two different laser-based therapies, i.e., photodynamic and photothermal therapy. ICG as photosensitizers (PS) has electrons in singlet ground state. When light is incident on it, absorption of photons leads to the movement of electrons to the excited states. Later on, it comes into the triplet state. The lifetime of the triplet state is in microseconds as compare to the singlet excited state that is of nanoseconds. Hence, it eventually forms singlet oxygen, and this reaction is called type II photochemical reaction. Sometimes, excited PS undergoes photochemical changes and leads to the formation of reactive oxygen. This phenomenon is called a type I photochemical reaction [64]. This is the mechanism of photosensitizers for photodynamic therapy. The work presented in this thesis is mainly focused on photothermal therapy. In photothermal therapy, when light is incident on cancer cell treated with photothermal agent, there will be heat generation that causes thermal expansion, an increase in pressure that ultimately leads to cell death. Anticancer photothermal agent is supposed to have a high wavelength absorbance band (far-red/ near-infrared) so that it can target deeply buried tumors. ICG is reported as one of the photothermal agent that can work in the NIR window.

2.3 Advantages and applications of ICG

To study the blood clots in tissue vasculature, NIR optical window has been used. However, the reflected signal from blood clots decreases as the depth of the clots increase[65,66]. This can be achieved by the use of ICG as it efficiently binds with the plasma proteins, mainly lipoproteins[66–68] that helps in studying the deeply buried inhomogeneities in the tissues. Additionally, ICG has been used in the clinical settings for the determination of cardiac output, liver malfunction, blood plasma volume,

localization of tumors,etc. [70]. It is being used as a wide variety of biomedical engineerings like peripheral tissue perfusion, angiography, photoacoustic imaging, photodynamic therapy, and photodynamic therapy, as shown in Figure 2.2.

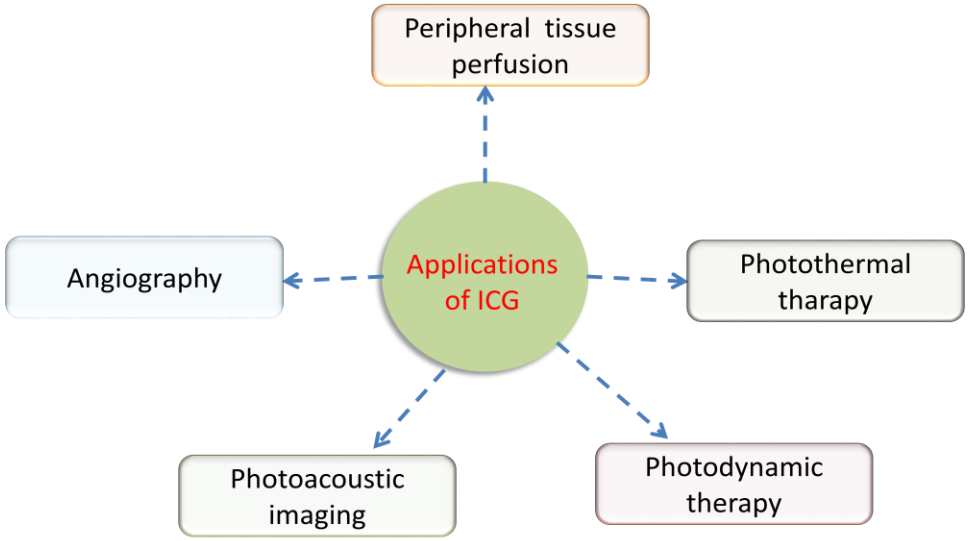

Figure 2.2 Applications of Indocyanine Green for clinical applications[71–74].

2.4 Limitations of ICG

Despite its clinical applications, ICG has shortcomings of non-specific targeting, rapid clearance (half-life is 2-4 minutes) through bile juice [76], hydrolytic instability[77], and poor photostability[78]. These limitations of ICG can be addressed by incorporating ICG within the nanoparticles to improve its half-life and stability in blood without interacting with serum proteins.

2.5 ICG encapsulated NP and its applications

ICG based NPs have been developed as a delivery system by using one of the characteristic properties of tumor blood vessels. This property of cancer is known as enhanced permeability retention effect (EPR)[75, 79–85]. ICG can be encapsulated into different NPs such as polymeric NP,

silica-based NP, magnetic NP, lipid-based NP, and many other NPs[86–96], as shown in Figure 2.3.

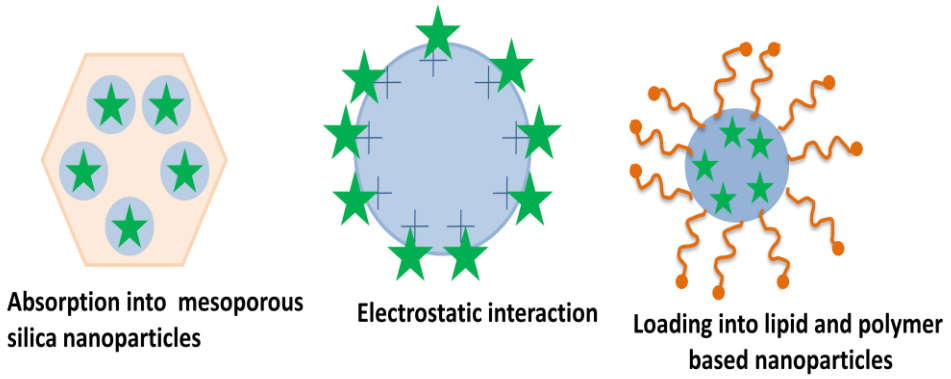

Figure 2.3 Illustration of three types of ICG nanoparticles- silica nanoparticles, magnetic nanoparticles, and polymeric nanoparticles[86–88].

Brief information about these nanoparticles are presented below:

2.5.1 ICG encapsulated lipid NP

Liposomes are one of the most common NP that is being used as a therapeutic agent. It is spherical vesicles consists of the natural or synthetic phospholipid bilayer. It has a unique property to encapsulate therapeutic as well as diagnosing agent either in lipid core or its interface[97]. It has been reported that on giving injection intradermally, ~50nm ICG encapsulated liposomes were started accumulating in lymph nodes only within 4 hours[87].

2.5.2 ICG encapsulated silica NP

Mesoporous silica (MS) NPs are highly porous with a large surface area. It can be functionalized to use in biomedical applications[98]. ICG is unable to get aggregated in MS NPs because of more surface area(93). Its elimination from the body is relying on the charge of MS-ICG-NPs, and it is not easily done.

2.5.3 ICG encapsulated polymeric NPs

These NPs are a major class of therapeutic carrier that is used in clinical applications. It can be fabricated by self-assembly method by using copolymers or macromolecules[97]. Poly (lactic-co-glycolic acid) is widely used biocompatible as well as biodegradable nanostructure encapsulated ICG that makes it suitable for the theranostic field. Zhao and his colleagues have synthesized ICG encapsulated PLGA-lecithin-polyethylene glycol under the size range of 200 nm. They have shown by using fluorescence imaging that free ICG was immediately excreted from the body whereas encapsulated ICG PLGA NP is retained inside the body for a longer time[90]. Hence, we can say that among all types of nanoparticles, polymeric nanoparticles are best suited for biomedical applications since it is biodegradable, biocompatible, and low immunogenicity.

2.6 ICG NPs for NIR imaging and cancer therapy

2.6.1 NIR imaging

ICG is encapsulated into nanocomposites consists of polymer and inorganic composites via covalent or non-covalent bond for NIR imaging. These NPs have shown more photostability, accumulation at tumor sites, biocompatibility, low aggregation, and high fluorescence as compared to free ICG. ICG encapsulation does not affect absorbance or fluorescence maxima but shows a change in intensity in comparison to free ICG. It could be useful for imaging sensitive and early-stage cancer diagnosis. NIR optical window is mostly used for guided imaging of margins of tumor and metastatic cancers[76]. Several types of ICG loaded nanoparticles are reported, such as magnetic carbon NP, lipid NP, metal organic NP, etc. These NPs are tabulated in Table 2 based on size, surface coating, and tumor type.

Table 2. ICG NPs for nearinfrared fluorescent imaging-guided photothermal therapy in cancer[76, 90, 107-110]

NP type	Size	Surface coating	Tumor type
Biomimetic	200.4 nm	Cancer cell membrane	Breast tumor
Magnetic carbon	10 nm	Bovine serum albumin	Breast tumor
Metal-organic	100 nm	Hyaluronic acid	Breast tumor
SPIO	27.4 nm	DSPE-PEG	Cervical carcinoma
Magnetite nanocluster	50-200 nm	Poly(dopamine)	Liver tumor
Lipid	20-40 nm	Folic acid	Breast tumor
PLGA	38, 69,116 nm	Polyethylene glycol	Pancreatic carcinoma

SPIO-superparamagnetic iron oxide; DSPE-PEG-1,2-distearoyl-sn-glycero-3-phosphoethanol-amine-N-[methoxy(polyethylene glycol)]; PLGA- poly(lactic-co-glycolic acid)

2.6.2 Photothermal therapy as cancer therapy

Photothermal therapy is being applied by using photothermal agent that generate heat through the non-radiative pathway and hence, used for thermal ablation of cancer cells[111]. These days photothermal therapy is evolved as a substitute for the treatment of cancer cell with minimum side-effects[112]. ICG is a suitable candidature to be used as a photothermal agent for PTT by using visible or NIR laser[76]. However, free ICG limited its usage as a photothermal agent for PTT due to its non-specificity, aggregation at higher concentration, less optical stability, etc. in vivo[113].

To overcome these limitations, ICG could be encapsulated within NPs that converts light energy of laser irradiation into heat that leads to thermal ablation of cancer cells. There are wide varieties of nanoparticles that have been used for PTT like gold NPs, graphene oxide NPs, carbon NPs, etc. but due to their low biodegradability and biocompatibility, we have emphasized on biopolymeric nanoparticles. Biopolymeric nanoparticles are suitable for PTT due to its versatile features like low immunogenicity, high biodegradability, and biocompatibility. Thus, nanoparticle mediated PTT might be useful over the conventional treatment method with minimal damage to surrounding normal tissues because it occurs only in the illuminated region[107,44,108].

Chapter 3

Objectives

Our main aim was to synthesize poly-L-lysine (PLL) nanoparticles encapsulating indocyanine green; an FDA approved NIR contrasting agent for photothermal therapy of cancer.

3.1 Objective 1

Our first goal was to fabricate ICG loaded poly-L-lysine nanoparticle through a two-step self-assembly process.

3.2 Objective 2

The second objective was to perform functional and morphological characterization of ICG-PLL NPs.

3.3 Objective 3

The third objective was to test the safety of ICG-PLL NPs using biological assay and in vitro cellular uptake of ICG-PLL NPs.

3.4 Objective 4

Our fourth objective was to compare the photothermal efficiency of free and nanoencapsulated ICG.

We hypothesized that the encapsulation of ICG into poly-L-lysine nanocarrier could increase the efficacy of photothermal therapy. The pictorial representation of the mechanism of photothermal therapy via ICG loaded PLL NP is shown in Figure 3. When laser light is irradiated on cancer cells treated with ICG-PLL NPs, heat is generated that causes a rise in temperature, thermal expansion, an increase in pressure that ultimately leads to cell death.

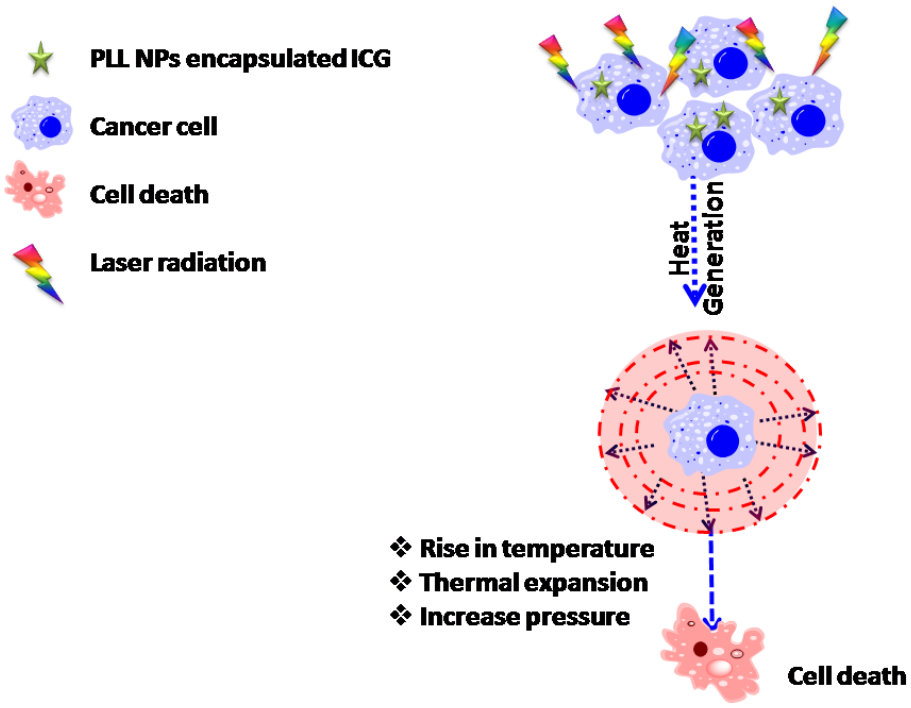

Figure 3 Schematic representation of hypothesis of ICG loaded nanoparticles for photothermal therapy of cancer.

Chapter 4

Materials, methods, and instrumentation

4.1 Materials

PLL (Molecular weight = 120 kDa, ~ 574 lysine unit, one HBr per lysine residual) was procured from Polysciences (Warrington, PA, USA). Tri-sodium citrate dihydrate was purchased from Merck (Darmstadt, Germany). Sodium phosphate dibasic heptahydrate and ICG were procured from Sigma Aldrich (St. Louis, MO, USA) and were used as received. The stock solutions of the chemicals were prepared in de-ionized (DI) water (Millipore 18.2 MΩ, Sartorius system) and stored at 4 degree Celsius.

Reagents of Phosphate buffered saline (PBS) like sodium chloride (NaCl), potassium chloride (KCl), disodium hydrogen phosphate (Na_2HPO_4), potassium dihydrogen phosphate (KH_2PO_4) were purchased from Thomas Baker (Mumbai). Dimethyl sulphoxide (DMSO) was procured from Merk (Darmstadt, Germany). MTT, paraformaldehyde, DAPI were procured from Hi-media (Mumbai). 10 × 2 mm quartz cuvette (Hellma GmbH & Co., Müllheim, Germany) is used for optical experiments.

Human cervical cancer cell line (HeLa), human liver cancer cell line (HUH7), human embryonic kidney cell line (HEK293T), human lung cancer cell line (A549) were procured from National Center for Cell Science (NCCS), Pune, India. Dulbecco's modified Eagle's medium, penstrap, fetal bovine serum was procured from Thermo Fisher (India) and used to prepare complete media to culture cell lines.

4.2 Methods and instrumentation

4.2.1 Preparation of nanoparticles

Poly-l-lysine is a polymer of basic amino acid, hence, positively charged and could react with negatively charged salts. The addition of tri-sodium citrate dihydrate and sodium phosphate dibasic heptahydrate, to the poly-L-lysine solution, caused the initial transparent polymer mixture to become turbid and cloudy, indicating aggregation of the positively charged polypeptide with the negatively charged salts. Afterward, on the addition of ICG, it permeates through aggregates of polymer and salt. Nanoparticleswere prepared by a two-step self-assembly method. At first, PLL was mixed with sodium citrate and sodium phosphate to which ICG was added, followed by making volume upto 1 mL using DI water, as shown in Figure 4.1.

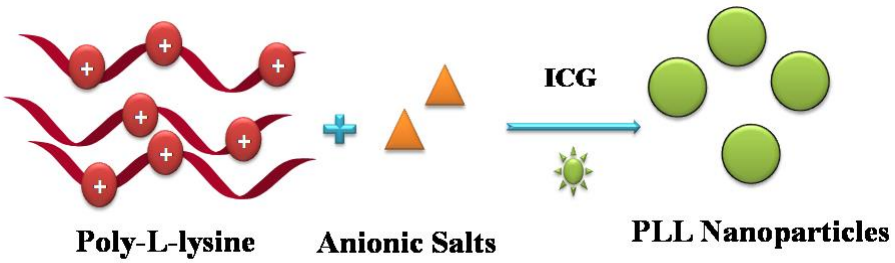

Figure 4.1 Schematic representation of the synthesis of nanoparticles.

Samples were then incubated for half an hour in the dark at room temperature. Differential centrifugation was done to pellet down the particles. This pellet was used for further characterization.

4.2.2 Preparation of reagents stock

4.2.2.1 Indocyanine green (ICG)

The stock concentration of ICG is 645 µM, was prepared by adding ICG powder in DI water and stored at -80˚C in dark condition to prevent thermal and photodegradation.

4.2.2.2 Phosphate buffered saline (PBS)

10X PBS stock was prepared by adding 80 g NaCl, 2 g KCl, 14.44 g Na_2HPO_4, 2.4 g KH_2PO_4, and pH was maintained to 7.4 by adding NaOH or HCl and stored at 4˚C. 1X PBS was used for experiments.

4.2.2.3 3-(4,5-dimethylthiazol-2-yl)-2,5-tetrazolium bromide (MTT)

5 mg of 3-(4,5-dimethylthiazol-2-yl)-2,5-tetrazolium bromide was added to 1 mL of 1X PBS.

4.2.2.4 Complete media

10% Heat-inactivated fetal bovine serum and 1% penicillin and streptomycin were added to 500 mL of Dulbecco's modified Eagle medium (DMEM) media to make it complete media.

4.2.3 Lyophilizer

Lyophilizer is also known as freeze dryer. It works on the principle of sublimation, where the frozen form of samples undergoes vapor without going into liquid phase under vacuum[114]. It consists of three stages: freezing phase, primary drying phase, and secondary drying phase. In the freezing phase, the temperature goes to below triple point to make sure that it follows sublimation inspite of melting for the cooling of the sample. It can help in preserving the physical form of the sample. In the primary drying phase, the pressure gets lower, and heat is given to the sample so that it gets sublimate. The vacuum also assists in sublimation[115]. 95% of water is sublimated in this stage. In the secondary drying phase, the temperature is raised higher than the primary drying stage so that bonds between water and sample get broken and ionically bound water gets removed. The fabricated nanoparticles were freeze-dried for electron microscopy measurements. Lyophilizer was used for drying the nanoparticles. For this purpose, 100 µL of DI water was added to the pellet of PLL NP and frozen into liquid nitrogen. Afterward, samples were

kept into the lyophilizer chamber, and water got sublimated in 12-13 hours.

4.2.4 Scanning Electron Microscope (SEM)

To study the morphology of the nanoparticles scanning electron microscopy was used. ICG-PLL NPs were prepared and lyophilized to characterize the morphology. Dried samples were coated with a thin layer of gold to make the samples conducting, on completion of gold coating, samples were kept on stub by using carbon tape and placed in the imaging chamber of field emission scanning electron microscope. (Supra 55 Zeiss).SEM is a type of microscopy that utilizes a focused beam of electrons of high energy which strikes on the sample and scans the same, hence, gives the information about topography, morphology, 3D image and size of the particle. Samples can be conducting or non-conducting. A metallic coating like gold or silver is required for non-conducting samples[116]. SEM mainly consists of a source of electrons, column down with electromagnetic lenses, electron detector, sample chamber, computer to view images. Electrons are produced at the top of the column and passed through a set of different electromagnetic lenses that strikes the surface of the sample. Samples are mounted on the stub and placed in a chamber that is evacuated by a pump[117,118]. On the interaction of electrons with the sample, it produces backscattered electrons, secondary electrons, etc. These electrons are detected by different detectors, and thus, image is produced on the screen of the desktop.

4.2.5 Dynamic Light Scattering (DLS)

The size and surface charge of the nanoparticles was also measured in an aqueous environment. Dynamic light scattering spectroscopy was used to determine the overall charge on the surface of particle and size in nanometer range by measuring the changes in the light intensity scattered through the colloidal solution or suspension. The liquid sample of ICG-

PLL NPs was sonicated before measurement. The nanoparticle size was determined as the averaged value of 50 runs. Hydrodynamic size and zeta potential were calculated by using a Nanoplussystem from Micrometrics Instrument Corporation. DLS is based on the principle of Brownian movement of suspended particles. Minute particles present in suspension move randomly in all direction. This zig-zag movement is called Brownian movement. Particles are moving randomly causes energy transfer to another particle to move. Hence, smaller particles can move at a higher speed than the larger one. The speed of the smaller particle is used to calculate the hydrodynamic diameter. The relation between hydrodynamic diameter and speed of the particle is given by the Stokes-Einstein equation[120].

$$D = k_в T/6\pi\eta R$$ where,

$k_в$ = Boltzmann constant, T = temperature, η = viscosity, R= Hydrodynamic radius

4.2.6 UV-Vis spectroscopy

UV-Vis spectrophotometer measures absorbance or transmittance. The main components of UV-Vis spectrophotometer are a source of light like deuterium lamp, monochromator, detector. The principle of UV-Vis spectrophotometer is based on Beer-Lambert law. According to this law, absorbance is proportional to the concentration of sample and path length of the cuvette (10×2 mm) traveled by light through the sample. When light is passed through the sample, the difference between incident light (I_o) and transmitted light (I) gives the amount of absorbed light[124].

The amount of transmitted light (T) is expressed as:

$T = I/I_0$ or $\% T = (I/I_0) \times 100$

The amount of absorbed light (A) is expressed as:

$A = -logT$

or

$A = \varepsilon Cl$ where, ε = extinction coefficient, C= concentration of sample, l= path length[125]

When optical energy is given to the molecule, photons are absorbed by electrons that results inan absorption spectrum[123]. This phenomenon can be explained by the Jablonski diagram as shown in Figure 4.2. The molecule can be in different rotational or vibrational states. By using UV-Vis spectrophotometer (Perkin Elmer), absorption spectra of free ICG and ICG-PLL NPs were taken from 190 nm to 1000 nm with 1 nm slit width and 480 nm/s scan speed.

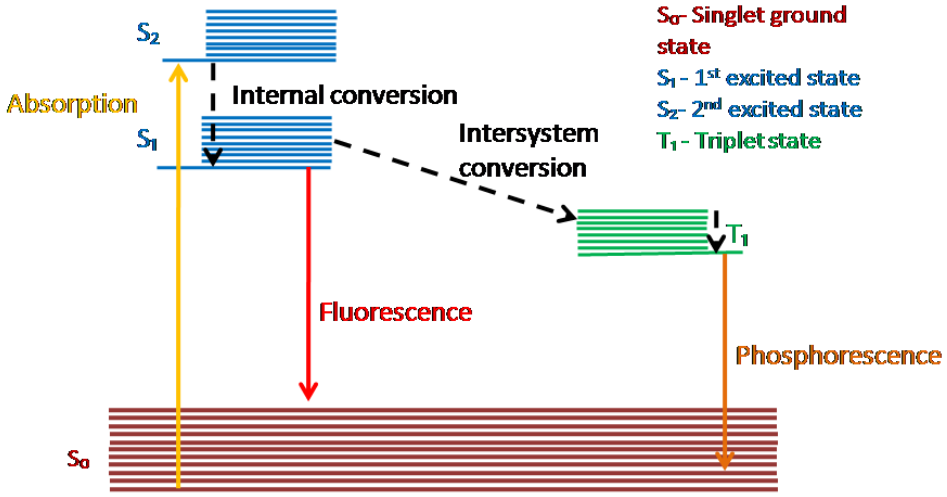

Figure 4.2 Excitation of a molecule is shown by Jablonski diagram.

4.2.7. Fluorescence spectroscopy

Fluorescence spectroscopy is based on the fluorescence phenomenon where the transition of electronsfrom a higher state to lower state. In this process, energy is emitted in the form of visible radiation. Photons are emitted at a higher wavelength than absorbed. The mechanism of fluorescence is shown by Jablonski diagram in Figure 4.2. Fluorescence

spectroscopy mainly consists ofa source of light- xenon lamp, two monochromators- one for tuning excitation wavelength and another one for fluorescence emission, sample holder, detectors. It is used to measure emission spectra by fixing excitation wavelength and scans the wavelength of emitted radiation via emission spectra. Fluorescence spectra of free ICG and encapsulated ICG were taken at excitation wavelength 680 nm and in the emission wavelength rangefrom 700 nm to 900 nm using fluorimeter (Jobin Yvon Horiba). The excitation and an emission slit width was 5 nm.

4.2.8 Cell viability assay with MTT

Cell viability assays are generally used to check the cytotoxicity ofdifferent drugs, chemicals, nanoparticles, etc. 3-(4,5-dimethylthiazol-2-yl)-2,5-tetrazoliumbromide (MTT) assay is one of most common quantitative colorimetric assay used for this purpose. Viable cells have mitochondrial enzyme NADPH dependent oxidoreductase enzyme that reduces yellow tetrazolium MTT to insoluble formazan purple crystals when incubated with viable cells. These crystals are dissolved on the addition of organic solvents like isopropanol or DMSO and quantified by taking absorbance at 570 nm in aplate reader. In our experiment, MTT assay was used to check the cellular viability of A549, HeLa, HUH7 cancer,and HEK293T normal cell lines after ICG-PLL NP incubation. 5×10^3cells/well were seeded in a 96-well flat bottom plate and grown in complete DMEM media for overnight. Then cells were treated with different concentration of free ICG and ICG-PLL NPs and incubated at 5% CO_2, 37˚C in a humidified incubator. On completion of 24 hours of treatment, 10µL of MTT (5mg/mL in PBS) was added and incubated for 4 hours in the incubator. Then 100 µL of DMSO was added, and absorbance was taken at 570 nm by a microplate reader. (Synergy H1 multi-mode)

4.2.9 Fluorescence microscopy

Fluorescence is most widely used contrast technique because it has a high signal to noise ratio for different applications. The light source is mercury or xenon lamp. Specific wavelength light is used to excite fluorophore present in the sample. Fluorescence microscope uses a combination of filters that are specific for excitation and emission wavelength of a particular fluorophore. Mainly three types of filter are present in this microscope excitation, dichromatic mirror, and emission filter. Detectors like CCD camera is used to image the emissionsignal.

For fluorescence imaging, HeLa 10^6 cells/well were seeded into 6-well flat bottom plates having rounded coverslip and kept for overnight to grow in the incubator. Cells were treated with different concentration of ICG and ICG-PLL NPs for 24 hours. Cells were washed with 1X PBS 2-3 times. 500 µL of 4% paraformaldehyde was added and incubated for 15 minutes. 500 µL of 0.5µg/mL DAPI was added and incubated for 5 minutes. Then 500 µL of 1X PBS was added in each well and covered the plate with aluminium foil. The slide was prepared by placing a coverslip on it and fixed with glycerol and studied using a fluorescence microscope.

4.2.10 Nd:YAG laser

Neodymium-doped yttrium aluminum garnet (Nd:YAG) laser mainly consists of the laser head, table-top controller, power supply. Nd:YAG laser is a pulsed, system comprises either two pump chambers with one flash lamp or one pump chamber with two flash lamps. This laser can work on three different wavelength- 1064 nm, 532 nm, 355 nm. The maximum power for 1064 nm, 532 nm, and 355 nm wavelengths are 4.4 W, 2.2 W, and 1.2 W respectively. This laser was used in Q-switch mode. The distance between the lens and the sample was 30 cm. The camera used for the photothermal experiment is FLIR DM285, 160 x120 resolution thermal imager. The schematic representation of this experiment is shown in Figure 4.3. This experiment is carried out to check the photothermal efficiency of free ICG and encapsulated ICG. Laser of

wavelength 532 nm was used for this experiment at 22˚C temperature. The 322.5 µM concentration of free ICG and four different concentration of ICG encapsulated PLL NPs were used under the laser, and the temperature rise was recorded for each sample for 60 seconds.

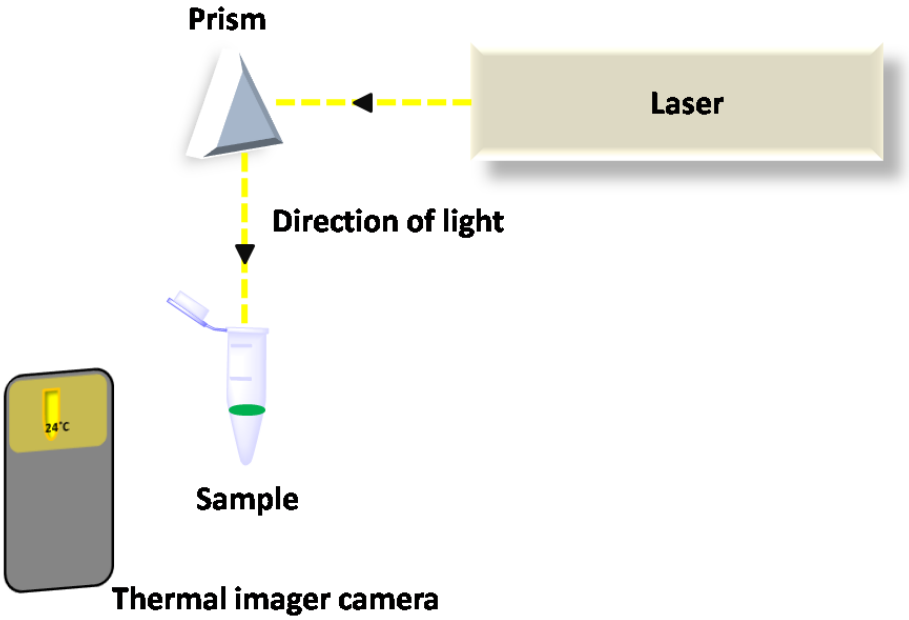

Figure 4.3 Schematic representation of laser experiment to check the photothermal efficacy of ICG loaded poly-L-lysine nanoparticles.

Chapter 5

Results and Discussion

ICG encapsulated PLL NPs were synthesized by a two-step self-assembly method, as shown in Figure 4.1. Briefly, PLL, salts (Tri-sodium citrate dehydrate and sodium phosphate dibasic heptahydrate) and ICG were mixed at room temperature to fabricate the ICG loaded nanoparticles. After 30 minutes of aging differential centrifugation was performed to obtain, ICG-PLL NPs in the pellet, as shown in Figure 5.1. After preparation of nanoparticles, morphological and optical studies were performed to determine the size, zeta potential, encapsulation of ICG into PLL NPs.

Figure 5.1 ICG-PLL NP pellet (encircled) after differential centrifugation.

5.1 Morphological characterization

Morphological characterization was performed to check the morphology of ICG-PLL NPs using a field-emission scanning electron microscope (FE-SEM) and dynamic light scattering (DLS) in the dry state and aqueous environment respectively.

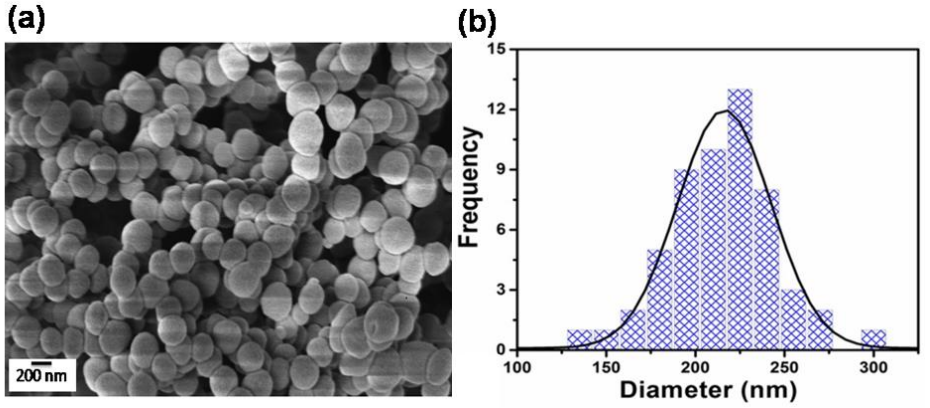

Figure 5.2 Morphological characterization of the PLL NPs (a) FE-SEM image of poly-l-lysine (PLL) NPs (b) Size distribution of PLL NPs.

The ICG-PLL NPs morphology was visualized under FE-SEM, and they were spherical, as shown in Figure 5.2(a). Further, the frequency distribution of the ICG-PLL NPs size was calculated with the help of Image J (NIH software), as shown in Figure 5.2(b). The mean diameter of these NPs was found to be ~225 nm, and these are nearly monodispersed in nature.

The hydrodynamic diameter of these NPs were measured by the dynamic light scattering (DLS) technique. The mean hydrodynamic diameter of the PLL NPs was ~275 nm, as shown in Figure 5.3 with 0.21 polydispersity index (PDI) that signifies that they are monodispersed in the aqueous environment. Further, the surface charge of these nanoparticles was measured by the zeta potential and was found to be +16 mV, suggesting that they are stable in an aqueous phase and do not undergo aggregation in aqueous media.

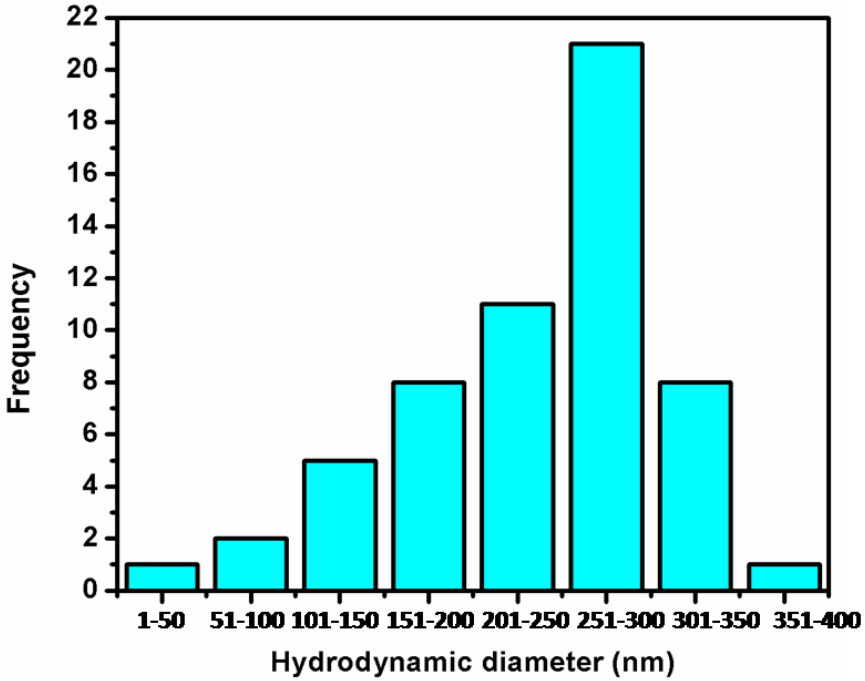

Figure 5.3 The hydrodynamic diameter of the PLL NPs measured by dynamic light scattering.

5.2 Optical characterization

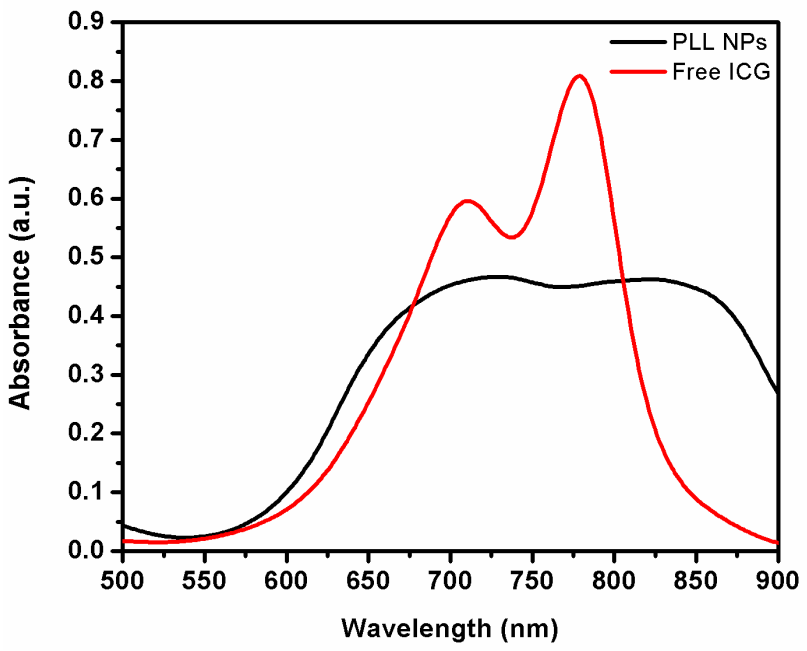

Figure 5.4 Absorption spectra of the PLL NPs and free ICG.

Spectroscopic analysis of the NPs was done by UV-Vis spectrophotometer and fluorimeter. Free ICG and ICG-PLL NPs exhibit absorption band in the range from 500 nm to 900 nm. ICG exhibits two characteristic absorption peaks around 780 nm and 715 nm, as shown in Figure 5.4. Absorption quenching and broadening of the absorption band was observed in the case of ICG-PLL NPs, which indicates the aggregation of the ICG molecules in the presence of a cationic polymer. The Absorption maxima of ICG is 780 nm. This is due to $S_0 \rightarrow S_1$ transition. Figure 5.5 shows the fluorescence emission from free ICG and ICG-PLL NPs. It can be observed that the intensity of free ICG is much higher than the nanoencapsulated ICG. This behaviour suggests the aggregation of ICG molecules in the presence of cationic polymer as indicated by the absorption data in Figure 5.4. Hence, the optical characterization confirmed that ICG is encapsulated into poly-L-lysine nanoparticles.

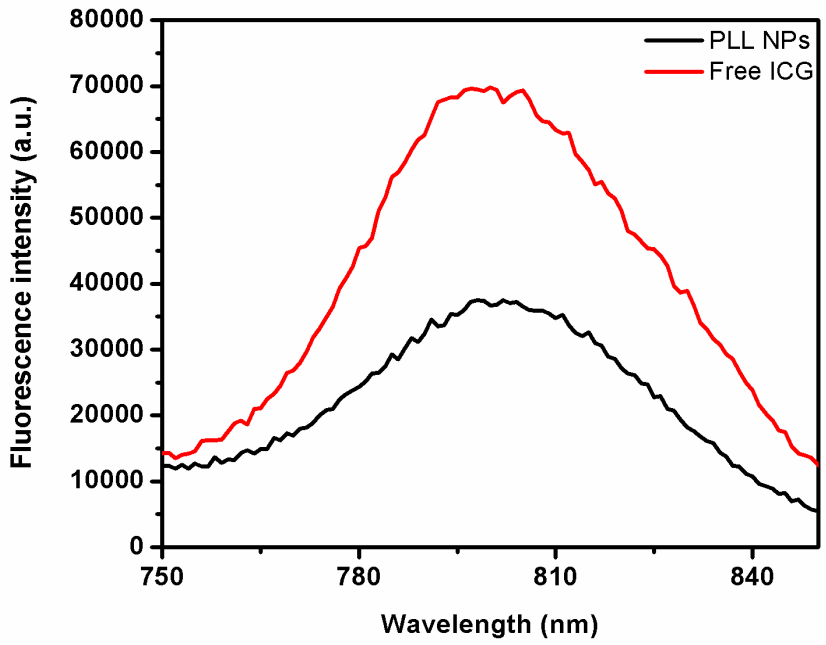

Figure 5.5 Emission spectra of the PLL NPs and free ICG by using fluorimeter.

5.3 Encapsulation efficiency of ICG

The ICG encapsulation efficiency of ICG-PLL NPs was calculated by dissolving the NPs pellet in DMSO and releasing the free ICG into the solution. The absorption of dissolved NPs was measured and compared with the calibration curve of free ICG absorption in DMSO. The encapsulation efficiency of ICG-PLL NPs was determined by the following formula:

Encapsulation efficiency = (ICG concentration after disintegration of NPs/ Initial concentration of ICG used) ×100.

λ max of ICG-DMSO absorption spectrum was observed around 778 nm. So, the absorbance of ICG encapsulated PLL NP on the addition of DMSO was recorded at 778 nm, and concentration was found 37 µM using the calibration curve of free ICG in DMSO.The calibration curve of ICG in solvent DMSO is shown in Figure 5.6. The encapsulation efficiency of ICG was found to be ~43%.

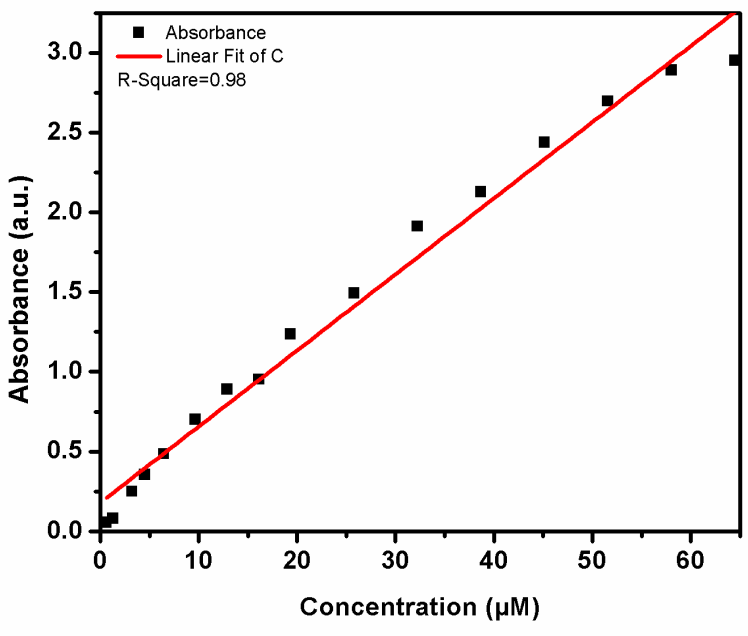

Figure 5.6 Calibration curve ofdifferent concentration of ICG in DMSO.

5.4 Optical stability of ICG encapsulated PLL NPs

Free ICG and PLL NPs were kept at 37˚C in ambient light to determine the photostability. The absorbance of both the samples was recorded at 778 nm (absorbance maxima) for 32 hours. As shown in Figure 5.7,

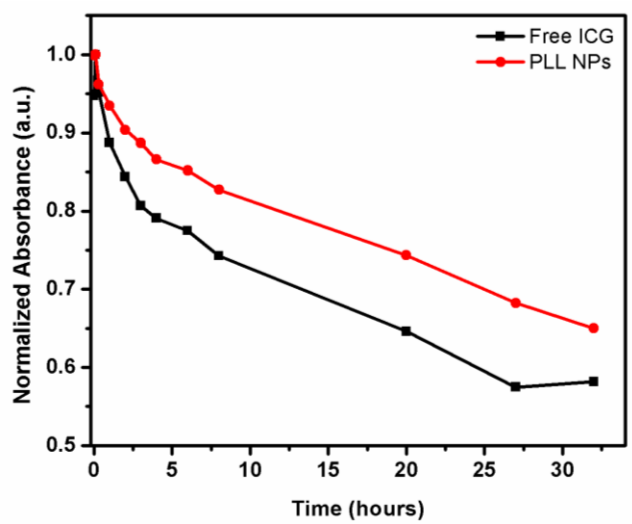

Figure 5.7 Comparision of stability of encapsulated ICG with free ICG at 37 degree Celsius.

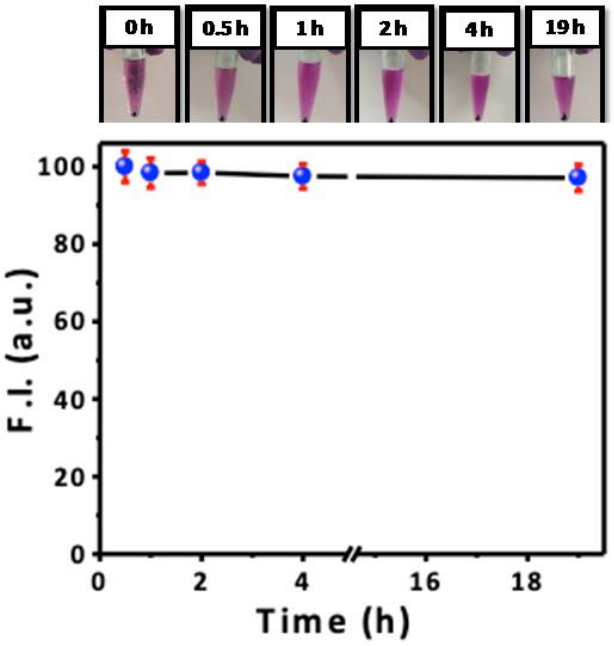

Figure 5.8 Release profile of ICG from ICG-PLL NPs at 37 degree Celsius in DMEM.

encapsulated ICG was found to be more stable than free ICG at 37-degree Celsius even in the presence of light. Hence, it suggests that ICG-PLL NPs protect better that its free form in light exposure. The release of ICG from ICG-PLL NPs was evaluated at physiological temperature i.e., 37-degree Celsius in Dulbecco's modified eagle medium (DMEM). As shown in Figure 5.8 also, it was observed that ICG-PLL NPs did not release any ICG in the medium till ~20 hours.

5.5 Assessment of cellular viability of PLL NPs

Biocompatibility and biodegradability are the key features of nanoparticles to be used inside the body. So, MTT assay was performed to determine the cytotoxic effect of ICG-PLL NPs in four different cell lines.

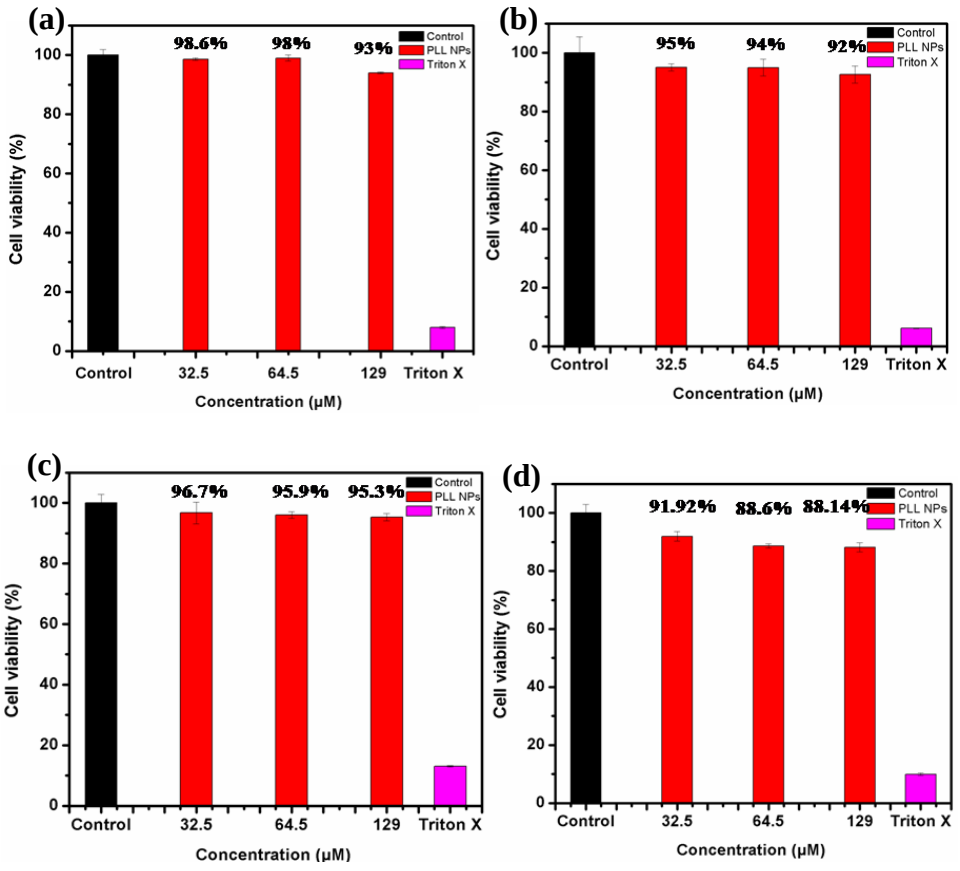

Figure 5.9 In vitro cellular viability assay of (a) A549, (b) HeLa (c) HUH7 and (d) HEK293T cell line.

Three cancerous cell line- HUH7, A549, HeLa, and one normal cell line- HEK293T were cultured. Untreated cells and Triton-X treated cells were kept as a negative and positive control, respectively. When A549 cells were treated with 5 µL (170 µg/mL), 10 µL (345 µg/mL), 20 µL (690 µg/mL) volume of polymer (stock concentration- 3.45 mg/mL) and 5 µL (3.45 µg/mL), 10 µL (6.9 µg/mL), 20 µL (13.8 µg/mL) volume of PLL NPs as shown in Figure. 5.9(a), 93-98% A549 cells were viable in both cases that depict that like polymer, ICG-PLL NPs are non-toxic to cells. Similarly, in the case of HeLa, HEK293T, HUH7 cells, as shown in Figure. 5.9(b), (c), (d), with different concentration of ICG-PLL NPs, cellular viability was found to be in the range of 88-98% even on nanoencapsulation. These data suggest that ICG-PLL NPs are safe for the cells and hence, could be used for biomedical applications.

5.6 Cellular uptake of ICG in vitro

For cellular uptake study, HeLa cells treated with free ICG and PLL NPs. Untreated cells were kept as a negative control.

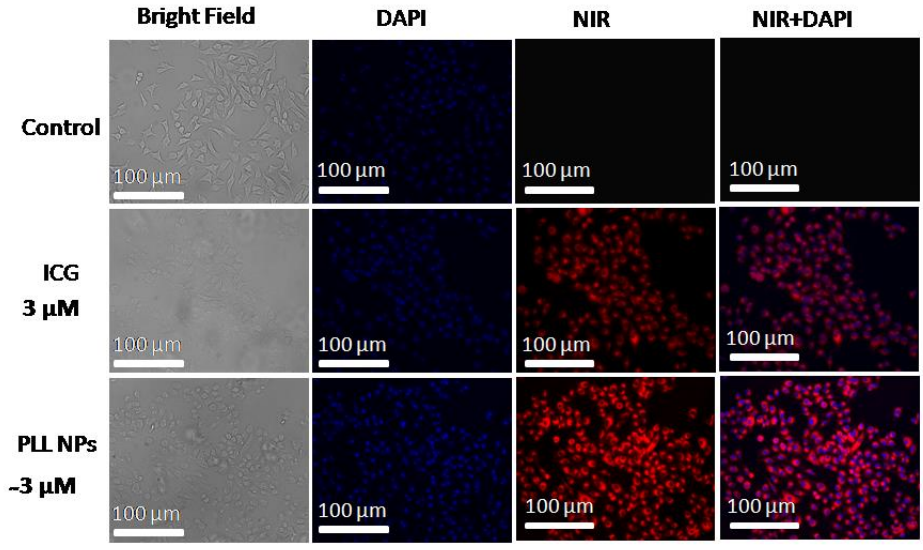

Figure 5.10 Cellular uptake of cells on treatment with free ICG and ICG encapsulated PLL NPs.

Bright field image, DAPI (for nucleus staining), NIR, NIR- DAPI merged image are shown in Figure 5.10 in a column first, second, third, fourth, respectively. It is observed in Figure. 5.10, cells treated with ICG encapsulated, PLL NPs have shown more fluorescence in comparison to free ICG that suggests that these NPs are capable of entering inside the cells effectively and thus ICG-PLL NPs could be utilized for bioimaging applications. Significant enhancement in fluorescence indicates that PLL NPs are capable of delivering ICG inside the cells in an efficient way.

5.7 Photothermal effect of free ICG and encapsulated ICG

Since ICG is a photothermal agent, it also shows the photothermal effect and could be effectively used for PTT. Free ICG and ICG-PLL NPs were used to determine the Photothermal effect by using a laser of wavelength 532 nm (Power density- 1.8 W/cm^2).

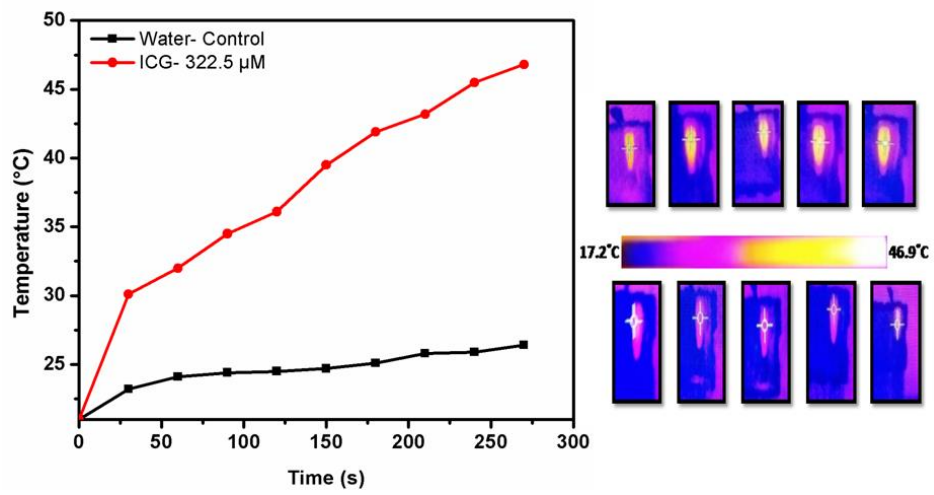

Figure 5.11 Effect of temperature on free ICG at laser power density 1.8 W/cm^2.

In Figure 5.11, it is clearly shown that within 5 minutes temperature rises to 46.9˚C that is enough to kill the cells. In the case of water, the temperature rises from 20.3˚C to 24.5˚C whereas temperature rises till 46.9˚C in case of free ICG when both are irradiated separately by laser.

Temperature measurement was recorded by a thermal imager camera. Three different concentrations of free ICG 322.5 µM (500 µL), 161.25 µM (250 µL) and 80.63 µM (125 µL) were used, and water was taken as control as represented in Figure 5.12. The photothermal profile of different volumes of ICG encapsulated PLL NPs are shown in Figure 5.13. Both experiments were performed at power density of 1.7 W/cm^2.

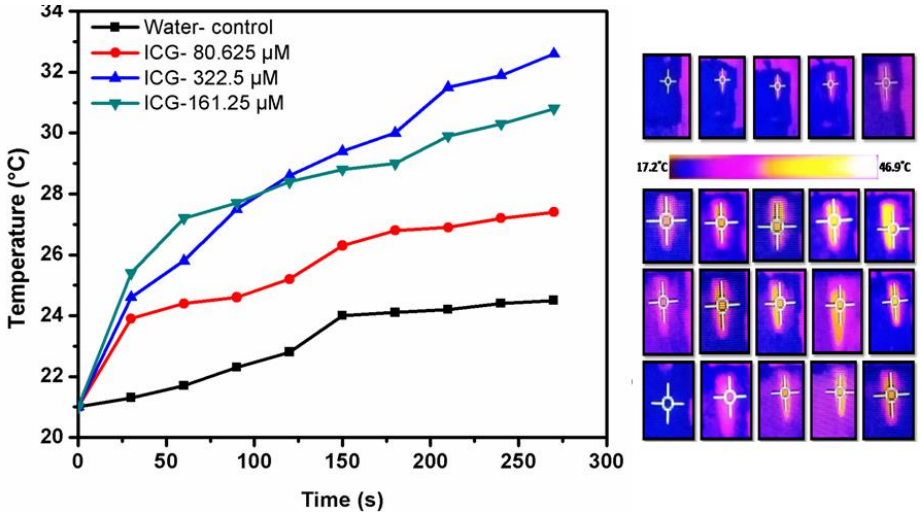

Figure 5.12 The photothermal effect of different amount of ICG at laser power density 1.7 W/cm^2.

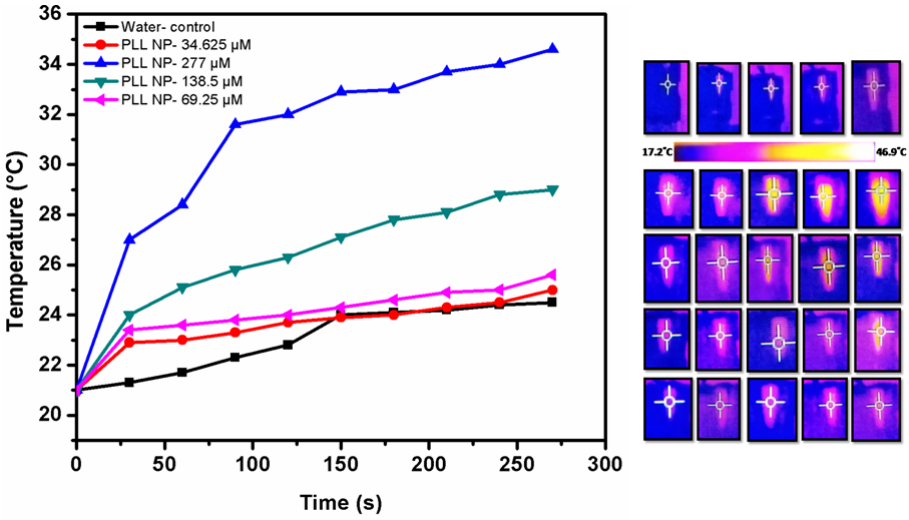

Figure 5.13 The photothermal effect of different amount of ICG encapsulated PLL NPs at laser power density 1.7 W/cm^2.

When the laser was irradiated for 5 minutes, the temperature rises with an increase in the volume of free ICG. The maximum temperature it achieved for free ICG volume 500 µL was 32.6˚C at power density 1.7 W/cm^2. However, it reached 34.5˚C when the laser was irradiated on 1000 µL of ICG-PLL NPs. Temperature is decreased with a decrease in the concentration of ICG-PLL NPs. These results suggest that ICG-PLL NPs efficiently show photothermal effect within five minutes only. These results suggest that ICG-PLL NPs can be used for photothermal effect in the visible wavelength range also.

Chapter 6

Conclusion and scope of future work

6.1 Conclusion

In summary, ICG encapsulating poly-L-lysine nanoparticles were successfully synthesized by a two-step self-assembly method at room temperature. SEM and DLS analysis confirmed that ICG encapsulated poly-L-lysine nanoparticles exhibit spherical morphology with an average size of 225 nm and zeta potential is +16 mV that depict its stability in the aqueous phase. The ICG loading efficiency was found to be ~43% in these NPs. These nanoparticles showed no cytotoxicity and are biocompatible and biodegradable. The ICG-PLL NPs show the photothermal effect.

6.2 Future scope

Development of ICG encapsulated PLL NPs can play an important role in the applications of the field of medicine. These NPs have shown the photothermal effect that can be useful in the photothermal therapy of cancer. In the future, these nanoparticles could be conjugated with targeting moieties, and their theranostic efficacy should be tested in an animal system.

REFERENCES

1. Siegel, R., Ma, J., Zou, Z., and Jemal, A. (2014) Cancer statistics, 2014. *CA. Cancer J. Clin.* **64**, 9–29

2. Bray, F., Ren, J.-S., Masuyer, E., and Ferlay, J. (2013) Global estimates of cancer prevalence for 27 sites in the adult population in 2008. *Int. J. Cancer*. **132**, 1133–1145

3. Ferlay, J., Shin, H.-R., Bray, F., Forman, D., Mathers, C., and Parkin, D. M. (2010) Estimates of worldwide burden of cancer in 2008: GLOBOCAN 2008. *Int. J. Cancer*. **127**, 2893–2917

4. Bray, F., Ferlay, J., Soerjomataram, I., Siegel, R. L., Torre, L. A., and Jemal, A. (2018) Global cancer statistics 2018: GLOBOCAN estimates of incidence and mortality worldwide for 36 cancers in 185 countries. *CA. Cancer J. Clin.***68**, 394–424

5. Ali, I., Wani, W., therapy, K. S.-C. (2011) Cancer Scenario in India with Future Perspectives. *J. Cancer Ther*. **8**, 56-70

6. Torre, L. A., Siegel, R. L., Ward, E. M., and Jemal, A. (2016) Global Cancer Incidence and Mortality Rates and Trends-An Update. *Cancer Epidemiol. Biomarkers Prev.***25**, 16–27

7. Jacob, B., and Gupta, P. C. (2008) A Nationally Representative Case-Control Study of Smoking and Death in India Worksite. *Chem. Commun.* **46**,1182-1184

8. *NATIONAL CANCER REGISTRY PROGRAMME Indian Council of Medical Research Three-Year Report of Population Based Cancer Registries Incidence and Distribution of Cancer (First Report of 20 PBCRs in India)* (2006)

9. Saranath, D., J, A. K.B. R. (2014) Current status of cancer burden:

global and Indian scenario. *researchgate.net*

10. Schroeder, A., Heller, D., Cancer, M. W. (2012) Treating metastatic cancer with nanotechnology. *nature.* **12**,39-50

11. Eckhardt, B., Francis, P., B. P. N. (2012) Strategies for the discovery and development of therapies for metastatic breast cancer. *nature.* **11**, 479-497

12. Zou, L., Wang, H., He, B., Zeng, L., Tan, T., Cao, H., X. H. (2016) Current approaches of photothermal therapy in treating cancer metastasis with nanotherapeutics. *ncbi.nlm.nih.gov*

13. Ferlay, J., Soerjomataram, I., Dikshit, R., Eser, S., Mathers, C., Rebelo, M., Parkin, D. M., Forman, D., and Bray, F. (2015) Cancer incidence and mortality worldwide: Sources, methods and major patterns in GLOBOCAN 2012. *Int. J. Cancer*. **136**, E359–E386

14. Tsugane, S., and Sasazuki, S. (2007) Diet and the risk of gastric cancer: review of epidemiological evidence. *Gastric Cancer*. **10**, 75–83

15. Trotti, A., Byhardt, R., Stetz, J., Gwede, C., Corn, B., Fu, K., Gunderson, L., McCormick, B., Morris, M., Rich, T., Shipley, W., and Curran, W. (2000) Common toxicity criteria: version 2.0. an improved reference for grading the acute effects of cancer treatment: impact on radiotherapy. *Int. J. Radiat. Oncol.***47**, 13–47

16. Miller, A. B., Hoogstraten, B., Staquet, M., and Winkler, A. (1981) Reporting results of cancer treatment. *Cancer*. **47**, 207–214

17. Chidambaram, M., Manavalan, R., and Kathiresan, K. (2011) Nanotherapeutics to Overcome Conventional Cancer Chemotherapy Limitations. *J. Pharm. Pharm. Sci.***14**, 67

18. Greish, K. (2010) Enhanced Permeability and Retention (EPR)

Effect for Anticancer Nanomedicine Drug Targeting. *Springer*.**624**, 25–37

19. Maeda, H., Wu, J., Sawa, T., Matsumura, Y., and Hori, K. (2000) Tumor vascular permeability and the EPR effect in macromolecular therapeutics: a review. *J. Control. Release*. **65**, 271–284

20. Maeda, H. (2001) SMANCS and polymer-conjugated macromolecular drugs: advantages in cancer chemotherapy. *Adv. Drug Deliv. Rev.***46**, 169–85

21. Iyer, A. K., Khaled, G., Fang, J., and Maeda, H. (2006) Exploiting the enhanced permeability and retention effect for tumor targeting. *Drug Discov. Today*. **11**, 812–818

22. Matsumura, Y., and Maeda, H. (1986) A new concept for macromolecular therapeutics in cancer chemotherapy: mechanism of tumoritropic accumulation of proteins and the antitumor agent smancs. *Cancer Res.***46**, 6387–92

23. Siegel, R. L., Miller, K. D., and Jemal, A. (2018) Cancer statistics, 2018. *CA. Cancer J. Clin.***68**, 7–30

24. Gradishar, W. J., Tjulandin, S., Davidson, N., Shaw, H., Desai, N., Bhar, P., Hawkins, M., and O'Shaughnessy, J. (2005) Phase III Trial of Nanoparticle Albumin-Bound Paclitaxel Compared With Polyethylated Castor Oil–Based Paclitaxel in Women With Breast Cancer. *J. Clin. Oncol.***23**, 7794–7803

25. Sabbatini, P., Aghajanian, C., Dizon, D., Anderson, S., Dupont, J., Brown, J. V., Peters, W. A., Jacobs, A., Mehdi, A., Rivkin, S., Eisenfeld, A. J., and Spriggs, D. (2004) Phase II Study of CT-2103 in Patients With Recurrent Epithelial Ovarian, Fallopian Tube, or Primary Peritoneal Carcinoma. *J. Clin. Oncol.***22**, 4523–4531

26. Bhatt, R., de Vries, P., Tulinsky, J., Bellamy, G., Baker, B., Singer, J. W., and Klein, P. (2003) Synthesis and in Vivo Antitumor Activity of Poly(l -glutamic acid) Conjugates of 20(*S*)-Camptothecin. *J. Med. Chem.***46**, 190–193

27. Li, C., and Wallace, S. (2008) Polymer-drug conjugates: recent development in clinical oncology. *Adv. Drug Deliv. Rev.***60**, 886–898

28. Seymour, L. W., Ferry, D. R., Anderson, D., Hesslewood, S., Julyan, P. J., Poyner, R., Doran, J., Young, A. M., Burtles, S., Kerr, D. J., and Cancer Research Campaign Phase I/II Clinical Trials committee (2002) Hepatic Drug Targeting: Phase I Evaluation of Polymer-Bound Doxorubicin. *J. Clin. Oncol.* **20**, 1668–1676

29. Batrakova, E., Dorodnych, T., Klinskii, E., Kliushnenkova, E., Shemchukova, O., Goncharova, O., Arjakov, S., Alakhov, V., and Kabanov, A. (1996) Anthracycline antibiotics non-covalently incorporated into the block copolymer micelles: in vivo evaluation of anti-cancer activity. *Br. J. Cancer*. **74**, 1545–1552

30. T. P., Balogh, L. P., Khan, M. K., and Baker, J. R. (2006) Development of the polymer micelle carrier system for doxorubicin.*Cancer Res.***75**, 6317–6324

31. Kim, T.-Y., Kim, D.-W., Chung, J.-Y., Shin, S. G., Kim, S.-C., Heo, D. S., Kim, N. K., and Bang, Y.-J. (2004) Phase I and Pharmacokinetic Study of Genexol-PM, a Cremophor-Free, Polymeric Micelle-Formulated Paclitaxel, in Patients with Advanced Malignancies. *Clin. Cancer Res.***10**, 3708–3716

32. Kukowska-Latallo, J. F., Candido, K. A., Cao, Z., Nigavekar, S. S., Majoros, I. J., Thomas, T. P., Balogh, L. P., Khan, M. K., and Baker, J. R. (2005) Nanoparticle Targeting of Anticancer Drug

Improves Therapeutic Response in Animal Model of Human Epithelial Cancer. *Cancer Res.***65**, 5317–5324

33. Malik, N., Evagorou, E. G., and Duncan, R. (1999) Dendrimer-platinate: a novel approach to cancer chemotherapy. *Anticancer. Drugs*. **10**, 767–776

34. Markman, M. (2006) Pegylated liposomal doxorubicin in the treatment of cancers of the breast and ovary. *Expert Opin. Pharmacother*.**7**, 1469–1474

35. Rivera, E. (2003) Current status of liposomal anthracycline therapy in metastatic breast cancer. *Clin. Breast Cancer*. **4 Suppl 2**, S76-83

36. Rosenthal, E., Poizot-Martin, I., Saint-Marc, T., Spano, J.-P., Cacoub, P., and DNX Study Group (2002) Phase IV study of liposomal daunorubicin (DaunoXome) in AIDS-related Kaposi sarcoma. *Am. J. Clin. Oncol.***25**, 57–9

37. Manchester, M., and Singh, P. (2006) Virus-based nanoparticles (VNPs): Platform technologies for diagnostic imaging. *Adv. Drug Deliv. Rev*.**58**, 1505–1522

38. Pastorin, G., Wu, W., Wieckowski, S., Briand, J.-P., Kostarelos, K., Prato, M., and Bianco, A. (2006) Double functionalisation of carbon nanotubes for multimodal drug delivery. *Chem. Commun.***65**, 1182-1184

39. Wu, W., Wieckowski, S., Pastorin, G., Benincasa, M., Klumpp, C., Briand, J.-P., Gennaro, R., Prato, M., and Bianco, A. (2005) Targeted Delivery of Amphotericin B to Cells by Using Functionalized Carbon Nanotubes. *Angew. Chemie Int. Ed.***44**, 6358–6362

40. Sheng, Z., Hu, D., Xue, M., He, M., Gong, P., and Cai, L. (2013)

Indocyanine Green Nanoparticles for Theranostic Applications. *Nano-Micro Lett.***5**, 145–150

41. Hirsch, L., Stafford, R., J. B. P. (2003) Nanoshell-mediated near-infrared thermal therapy of tumors under magnetic resonance guidance. *Natl. Acad Sci.***100**, 13549-13554

42. Chu, K., Cancer, D. D. N. R. (2014) Thermal ablation of tumours: biological mechanisms and advances in therapy. *nature.***14**, 199-208

43. Hwang, S., Nam, J., Jung, S., Song, J., Doh, H., and Kim, S. (2014) Gold nanoparticle-mediated photothermal therapy: current status and future perspective. *Nanomedicine*. **9**, 2003–2022

44. Song, S., Shen, H., Yang, T., Wang, L., Fu, H., Chen, H., and Zhang, Z. (2017) Indocyanine Green Loaded Magnetic Carbon Nanoparticles for Near Infrared Fluorescence/Magnetic Resonance Dual-Modal Imaging and Photothermal Therapy of Tumor. *ACS Appl. Mater. Interfaces*. **9**, 9484–9495

45. Xiaohua Huang, Ivan H. El-Sayed, Wei Qian and Mostafa A. El-Sayed. (2006) Cancer Cell Imaging and Photothermal Therapy in the Near-Infrared Region by Using Gold Nanorods. *J. Am. Chem. Soc*. **128**, 2115-2120

46. Meijering, E., Dzyubachyk, O., Smal, I., and van Cappellen, W. A. (2009) Tracking in cell and developmental biology. *Semin. Cell Dev. Biol.***20**, 894–902

47. Weissleder, R. (2001) A clearer vision for in vivo imaging. *Nat. Biotechnol.***19**, 316–317

48. Kumari, A., and Gupta, S. (2019) Two-photon excitation and direct emission from S_2 state of U.S. Food and Drug Administration approved near-infrared dye: Application of anti-Kasha's rule for

two-photon fluorescence imaging. *J. Biophotonics*. **12**, e201800086

49. Dolmans, D. E. J. G. J., Fukumura, D., and Jain, R. K. (2003) Photodynamic therapy for cancer. *Nat. Rev. Cancer*. **3**, 380–387

50. Peng Zhang, Wim Steelant, Manoj Kumar, and, and Scholfield†, M. (2007) Versatile Photosensitizers for Photodynamic Therapy at Infrared Excitation. *J. Am. Chem. Soc.***129**, 4526-4527

51. Luo, S., Zhang, E., Su, Y., Cheng, T., and Shi, C. (2011) A review of NIR dyes in cancer targeting and imaging. *Biomaterials*. **32**, 7127–7138

52. Mordon, S., Devoisselle, J., S. S. B. M. (1998) Indocyanine green: physicochemical factors affecting its fluorescencein vivo. *Elsevier*. **55**, 146-152

53. Dzurinko, V., Gurwood, A., Association, J. P. A. O. (2004) Intravenous and indocyanine green angiography. *Elsevier.***75**, 743-755

54. Desmettre, T., Devoisselle, J., ophthalmology, S. M.-S. (2000) Fluorescence properties and metabolic features of indocyanine green (ICG) as related to angiography. *Elsevier*. **45**, 15-27

55. Björnsson, Ó. G., Murphy, R., and Chadwick, V. S. (1982) Physicochemical studies of indocyanine green (ICG): absorbance/concentration relationship, pH tolerance and assay precision in various solvents. *Experientia*. **38**, 1441–1442

56. Engel, E., Schraml, R., Maisch, T. (2008) Light-induced decomposition of indocyanine green. *arvojournals.org*

57. Mishra, A., Behera, R. K., Behera, P. K., Mishra, B. K., and Behera, G. B. (2000) Cyanines during the 1990s: A Review. *Chem. Rev.***100**, 1973–2012

58. Landsman, M. L., Kwant, G., Mook, G. A., and Zijlstra, W. G. (1976) Light-absorbing properties, stability, and spectral stabilization of indocyanine green. *J. Appl. Physiol.***40**, 575–583

59. Landsman, M. L., Kwant, G., Mook, G. A., and Zijlstra, W. G. (1976) Light-absorbing properties, stability, and spectral stabilization of indocyanine green. *J. Appl. Physiol.***40**, 575–583

60. Xu, Q., Heo, C. H., Kim, J. A., Lee, H. S., Hu, Y., Kim, D., Swamy, K. M. K., Kim, G., Nam, S.-J., Kim, H. M., and Yoon, J. (2016) A Selective Imidazoline-2-thione-Bearing Two-Photon Fluorescent Probe for Hypochlorous Acid in Mitochondria. *Anal. Chem.***88**, 6615–6620

61. Proc, F. I. M. C. (1960) Indocyanine green : physical and physiologic properties.*Science.* **132**, 104-109

62. Gathje, J., Steuer, R. R., and Nicholes, K. R. (1970) Stability studies on indocyanine green dye. *J. Appl. Physiol.***29**, 181–185

63. Alander, J. T., Kaartinen, I., Laakso, A., Pätilä, T., Spillmann, T., Tuchin, V. V., Venermo, M., and Välisuo, P. (2012) A Review of Indocyanine Green Fluorescent Imaging in Surgery. *Int. J. Biomed. Imaging*. **2012**, 1–26

64. Foote, C. S. (1968) Mechanisms of photosensitized oxidation. There are several different types of photosensitized oxidation which may be important in biological systems. *Science*. **162**, 963–970

65. Kuroda, K., Kinouchi, H., Kanemaru. (2011) Indocyanine green videoangiography to detect aneurysm and related vascular structures buried in subarachnoid clots: case report. *J. Neurosurg.* **114**, 1054-1059

66. Nussbaum, E. S., Defillo, A., and Nussbaum, L. (2012) The Use of

Indocyanine Green Videoangiography to Optimize the Dural Opening for Intracranial Parasagittal Lesions. *Oper. Neurosurg.***70**, 61-68

67. Baker, K. J. (1966) Binding of Sulfobromophthalein (BSP) Sodium and Indocyanine Green (ICG) by Plasma 1 Lipoproteins. *Exp. Biol. Med.***122**, 957–963

68. Kamisaka, K., Yatsuji, Y., Yamada, H., and Kameda, H. (1974) The binding of indocyanine green and other organic anions to serum proteins in liver diseases. *Clin. Chim. Acta*. **53**, 255–264

69. Yoneya, S., Saito, T., science, Y. K. (1998) Binding properties of indocyanine green in human blood. *iovs.arvojournals.org*. **39**, 1286-1290

70. Maarek, J.-M. I., Holschneider, D. P., and Harimoto, J. (2001) Fluorescence of indocyanine green in blood: intensity dependence on concentration and stabilization with sodium polyaspartate. *J. Photochem. Photobiol. B Biol.***65**, 157–164

71. Lev, A., Kotler, Z., and Sfez, B. G. (2000) Ultrasound tagged light imaging in turbid media in a reflectance geometry. *Opt. Lett.***25**, 378

72. Tuchin, V. V., Genina, E. A., Bashkatov, A. N., Simonenko, G. V., Odoevskaya, O. D., and Altshuler, G. B. (2003) A pilot study of ICG laser therapy ofacne vulgaris: Photodynamic and photothermolysis treatment. *Lasers Surg. Med.***33**, 296–310

73. Kang, Y., Lee, J., Kwon, K., and Choi, C. (2010) Application of novel dynamic optical imaging for evaluation of peripheral tissue perfusion. *Int. J. Cardiol.***145**, e99–e101

74. Newman, M., and Samson, M. (2009) The Application of Laser-Assisted Indocyanine Green Fluorescent Dye Angiography in

Microsurgical Breast Reconstruction. *J. Reconstr. Microsurg.***25**, 021–026

75. Patz, A., Flower, R. W., Klein, M. L., Orth, D. H., Fleischman, J. A., and Mcleod, S. (1976) Clinical Application of Indocyanine Green Angiography. Springer, Dordrecht. **9**, 245–251

76. Zheng, M., Zhao, P., Luo, Z., Gong, P., Zheng, C., Zhang, P., Yue, C., Gao, D., Ma, Y., and Cai, L. (2014) Robust ICG Theranostic Nanoparticles for Folate Targeted Cancer Imaging and Highly Effective Photothermal Therapy. *ACS Appl. Mater. Interfaces*. **6**, 6709–6716

77. Wu, L., Fang, S., Shi, S., Deng, J., Liu, B., and Cai, L. (2013) Hybrid Polypeptide Micelles Loading Indocyanine Green for Tumor Imaging and Photothermal Effect Study. *Biomacromolecules*. **14**, 3027–3033

78. Wang, Y.W., Fu, Y.Y., Peng, Q., Guo, S.S., Liu, G., Li, J., Yang, H.-H., and Chen, G.-N. (2013) Dye-enhanced graphene oxide for photothermal therapy and photoacoustic imaging. *J. Mater. Chem. B*. **1**, 5762

79. Mok, H., Jeong, H., Kim, S.-J., and Chung, B. H. (2012) Indocyanine green encapsulated nanogels for hyaluronidase activatable and selective near infrared imaging of tumors and lymph nodes. *Chem. Commun.***48**, 8628-8634

80. Wan, Z., Mao, H., Guo, M., Li, Y., Zhu, A., Yang, H., He, H., Shen, J., Zhou, L., Jiang, Z., Ge, C., Chen, X., Yang, X., Liu, G., and Chen, H. (2014) Highly efficient hierarchical micelles integrating photothermal therapy and singlet oxygen-synergized chemotherapy for cancer eradication. *Theranostics*. **4**, 399–411

81. Ma, Y., Sadoqi, M., and Shao, J. (2012) Biodistribution of

indocyanine green-loaded nanoparticles with surface modifications of PEG and folic acid. *Int. J. Pharm.***436**, 25–31

82. Patel, R. H., Wadajkar, A. S., Patel, N. L., Kavuri, V. C., Nguyen, K. T., and Liu, H. (2012) Multifunctionality of indocyanine green-loaded biodegradable nanoparticles for enhanced optical imaging and hyperthermia intervention of cancer. *J. Biomed. Opt.***17**, 046003

83. Zheng, M., Yue, C., Ma, Y., Gong, P., Zhao, P., Zheng, C., Sheng, Z., Zhang, P., Wang, Z., and Cai, L. (2013) Single-Step Assembly of DOX/ICG Loaded Lipid–Polymer Nanoparticles for Highly Effective Chemo-photothermal Combination Therapy. *ACS Nano*. **7**, 2056–2067

84. Saxena, V., Sadoqi, M., and Shao, J. (2004) Indocyanine green-loaded biodegradable nanoparticles: preparation, physicochemical characterization and in vitro release. *Int. J. Pharm.***278**, 293–301

85. Zhong, J., Yang, S., Zheng, X., Zhou, T., and Xing, D. (2013) *In vivo* photoacoustic therapy with cancer-targeted indocyanine green-containing nanoparticles. *Nanomedicine*. **8**, 903–919

86. Yaseen, M. A., Yu, J., Jung, B., Wong, M. S., and Anvari, B. (2009) Biodistribution of Encapsulated Indocyanine Green in Healthy Mice. *Mol. Pharm.***6**, 1321–1332

87. Gravier, J., Navarro, F. P., Delmas, T., Mittler, F., Couffin, A.-C., Vinet, F., and Texier, I. (2011) Lipidots: competitive organic alternative to quantum dots for in vivo fluorescence imaging. *J. Biomed. Opt.***16**, 096013

88. Sayag, D., Cabon, Q., Texier, I., Navarro, F. P., Boisgard, R., Virieux-Watrelot, D., Carozzo, C., and Ponce, F. (2016) Phase-0/phase-I study of dye-loaded lipid nanoparticles for near-infrared fluorescence imaging in healthy dogs. *Eur. J. Pharm.*

*Biopharm.***100**, 85–93

89. Mérian, J., Boisgard, R., Bayle, P.-A., Bardet, M., Tavitian, B., and Texier, I. (2015) Comparative biodistribution in mice of cyanine dyes loaded in lipid nanoparticles. *Eur. J. Pharm. Biopharm.***93**, 1–10

90. Zhao, P., Zheng, M., Yue, C., Luo, Z., Gong, P., Gao, G., Sheng, Z., Zheng, C., and Cai, L. (2014) Improving drug accumulation and photothermal efficacy in tumor depending on size of ICG loaded lipid-polymer nanoparticles. *Biomaterials*. **35**, 6037–6046

91. Beziere, N., Lozano, N., Nunes, A., Salichs, J., Queiros, D., Kostarelos, K., and Ntziachristos, V. (2015) Dynamic imaging of PEGylated indocyanine green (ICG) liposomes within the tumor microenvironment using multi-spectral optoacoustic tomography (MSOT). *Biomaterials*. **37**, 415–424

92. Bahmani, B., Lytle, C. Y., Walker, A. M., Gupta, S., Vullev, V. I., and Anvari, B. (2013) Effects of nanoencapsulation and PEGylation on biodistribution of indocyanine green in healthy mice: quantitative fluorescence imaging and analysis of organs. *Int. J. Nanomedicine*. **8**, 1609–20

93. Lee, C.-H., Cheng, S.-H., Wang, Y.-J., Chen, Y.-C., Chen, N.-T., Souris, J., Chen, C.-T., Mou, C.-Y., Yang, C.-S., and Lo, L.-W. (2009) Near-Infrared Mesoporous Silica Nanoparticles for Optical Imaging: Characterization and In Vivo Biodistribution. *Adv Funct Mater*. **19**, 215–222

94. Souris, J. S., Lee, C.-H., Cheng, S.-H., Chen, C.-T., Yang, C.-S., Ho, J. A., Mou, C.-Y., and Lo, L.-W. (2010) Surface charge-mediated rapid hepatobiliary excretion of mesoporous silica nanoparticles. *Biomaterials*. **31**, 5564–5574

95. Huang, J., Shu, Q., Wang, L., Wu, H., Wang, A. Y., and Mao, H. (2015) Layer-by-layer assembled milk protein coated magnetic nanoparticle enabled oral drug delivery with high stability in stomach and enzyme-responsive release in small intestine. *Biomaterials*. **39**, 105–113

96. Ashokan, A., Gowd, G. S., Somasundaram, V. H., Bhupathi, A., Peethambaran, R., Unni, A. K. K., Palaniswamy, S., Nair, S. V., and Koyakutty, M. (2013) Multifunctional calcium phosphate nano-contrast agent for combined nuclear, magnetic and near-infrared in vivo imaging. *Biomaterials*. **34**, 7143–7157

97. Luk, B. T., Fang, R. H., and Zhang, L. (2012) Lipid- and polymer-based nanostructures for cancer theranostics. *Theranostics*. **2**, 1117–26

98. Slowing, I. I., Trewyn, B. G., Giri, S., and Lin, V. S.-Y. (2007) Mesoporous Silica Nanoparticles for Drug Delivery and Biosensing Applications. *Adv. Funct. Mater.***17**, 1225–1236

99. Altınoğlu, E. I., Russin, T. J., Kaiser, J. M., Barth, B. M., Eklund, P. C., Kester, M., and Adair, J. H. (2008) Near-Infrared Emitting Fluorophore-Doped Calcium Phosphate Nanoparticles forIn Vivo Imaging of Human Breast Cancer. *ACS Nano*. **2**, 2075–2084

100. Barth, B. M., Sharma, R., Altınoğlu, E. İ., Morgan, T. T., Shanmugavelandy, S. S., Kaiser, J. M., McGovern, C., Matters, G. L., Smith, J. P., Kester, M., and Adair, J. H. (2010) Bioconjugation of Calcium Phosphosilicate Composite Nanoparticles for Selective Targeting of Human Breast and Pancreatic Cancers *In Vivo*. *ACS Nano*. **4**, 1279–1287

101. Tsuchimochi, M., Hayama, K., Toyama, M., Sasagawa, I., and Tsubokawa, N. (2013) Dual-modality imaging with 99mTc and

fluorescent indocyanine green using surface-modified silica nanoparticles for biopsy of the sentinel lymph node: an animal study. *EJNMMI Res.***3**, 33

102. Yamaguchi, H., Tsuchimochi, M., Hayama, K., Kawase, T., Tsubokawa, N., Yamaguchi, H., Tsuchimochi, M., Hayama, K., Kawase, T., and Tsubokawa, N. (2016) Dual-Labeled Near-Infrared/99mTc Imaging Probes Using PAMAM-Coated Silica Nanoparticles for the Imaging of HER2-Expressing Cancer Cells. *Int. J. Mol. Sci.***17**, 1086

103. Zeng, C., Shang, W., Wang, K., Chi, C., Jia, X., Fang, C., Yang, D., Ye, J., Fang, C., and Tian, J. (2016) Intraoperative Identification of Liver Cancer Microfoci Using a Targeted Near-Infrared Fluorescent Probe for Imaging-Guided Surgery. *Sci. Rep.***6**, 21959

104. Kim, T. H., Chen, Y., Mount, C. W., Gombotz, W. R., Li, X., and Pun, S. H. (2010) Evaluation of Temperature-Sensitive, Indocyanine Green-Encapsulating Micelles for Noninvasive Near-Infrared Tumor Imaging. *Pharm. Res.***27**, 1900–1913

105. Zheng, C., Zheng, M., Gong, P., Jia, D., Zhang, P., Shi, B., Sheng, Z., Ma, Y., and Cai, L. (2012) Indocyanine green-loaded biodegradable tumor targeting nanoprobes for in vitro and in vivo imaging. *Biomaterials*. **33**, 5603–5609

106. Tsujimoto, H., Morimoto, Y., Takahata, R., Nomura, S., Yoshida, K., Horiguchi, H., Hiraki, S., Ono, S., Miyazaki, H., Saito, D., Hara, I., Ozeki, E., Yamamoto, J., and Hase, K. (2014) Photodynamic therapy using nanoparticle loaded with indocyanine green for experimental peritoneal dissemination of gastric cancer. *Cancer Sci.***105**, 1626–1630

107. Chen, Z., Zhao, P., Luo, Z., Zheng, M., Tian, H., Gong, P., Gao, G.,

Pan, H., Liu, L., Ma, A., Cui, H., Ma, Y., and Cai, L. (2016) Cancer Cell Membrane–Biomimetic Nanoparticles for Homologous-Targeting Dual-Modal Imaging and Photothermal Therapy. *ACS Nano*. **10**, 10049–10057

108. Cai, W., Gao, H., Chu, C., Wang, X., Wang, J., Zhang, P., Lin, G., Li, W., Liu, G., and Chen, X. (2017) Engineering Phototheranostic Nanoscale Metal–Organic Frameworks for Multimodal Imaging-Guided Cancer Therapy. *ACS Appl. Mater. Interfaces*. **9**, 2040–2051

109. Ma, Y., Tong, S., Bao, G., Gao, C., and Dai, Z. (2013) Indocyanine green loaded SPIO nanoparticles with phospholipid-PEG coating for dual-modal imaging and photothermal therapy. *Biomaterials*. **34**, 7706–7714

110. Wu, M., Wang, Q., Zhang, D., Liao, N., Wu, L., Huang, A., and Liu, X. (2016) Magnetite nanocluster@poly(dopamine)-PEG@ indocyanine green nanobead with magnetic field-targeting enhanced MR imaging and photothermal therapy in vivo. *Colloids Surfaces B Biointerfaces*. **141**, 467–475

111. Yue, C., Liu, P., Zheng, M., Zhao, P., Wang, Y., Ma, Y., and Cai, L. (2013) IR-780 dye loaded tumor targeting theranostic nanoparticles for NIR imaging and photothermal therapy. *Biomaterials*. **34**, 6853–6861

112. Wu, M., Wang, Q., Zhang, D., Liao, N., Wu, L., … A. H.-C. and S. B. (2016) Magnetite nanocluster@ poly (dopamine)-PEG@ indocyanine green nanobead with magnetic field-targeting enhanced MR imaging and photothermal therapy in vivo. *Elsevier.***1**, 467-475

113. Zheng, X., Zhou, F., Wu, B., Chen, W. R., and Xing, D. (2012)

Enhanced Tumor Treatment Using Biofunctional Indocyanine Green-Containing Nanostructure by Intratumoral or Intravenous Injection. *Mol. Pharm.***9**, 514–522

114. Zhai, S., Su, H., Taylor, R., and Slater, N. K. H. (2005) Pure ice sublimation within vials in a laboratory lyophiliser; comparison of theory with experiment. *Chem. Eng. Sci.***60**, 1167–1176

115. Naidoo, D., and Pratt, O. E. (1954) A freeze drying apparatus for neurohistochemical work. *Vacuum*. **4**, 195–197

116. von Ardenne, M. (1938) Das Elektronen-Rastermikroskop. *Zeitschrift für Phys.***109**, 553–572

117. Robinson, V. N. E. (1975) The elimination of charging artefacts in the scanning electron microscope. *J. Phys. E.***8**, 638–640

118. Moncrieff, D. A., Robinson, V. N. E., and Harris, L. B. (1978) Charge neutralisation of insulating surfaces in the SEM by gas ionisation. *J. Phys. D. Appl. Phys.***11**, 2315–2325

119. Miller, C. C. (1924) The Stokes-Einstein Law for Diffusion in Solution. *Proc. R. Soc. A Math. Phys. Eng. Sci.***106**, 724–749

120. Bigio, I. J., and Mourant, J. R. (1997) Ultraviolet and visible spectroscopies for tissue diagnostics: fluorescence spectroscopy and elastic-scattering spectroscopy. *Phys. Med. Biol.***42**, 803–814

121. Batistela, V. R., Pellosi, D. S., de Souza, F. D., da Costa, W. F., de Oliveira Santin, S. M., de Souza, V. R., Caetano, W., de Oliveira, H. P. M., Scarminio, I. S., and Hioka, N. (2011) pKa determinations of xanthene derivates in aqueous solutions by multivariate analysis applied to UV–Vis spectrophotometric data. *Spectrochim. Acta Part A Mol. Biomol. Spectrosc.***79**, 889–897

122. Lichtenthaler, H. K., and Buschmann, C. (2001) Chlorophylls and

Carotenoids: Measurement and Characterization by UV-VIS Spectroscopy. *Curr. Protoc. Food Anal. Chem.***1**, F4.3.1-F4.3.8

123. Hobbie, J. E., Daley, R. J., and Jasper, S. (1977) Use of nuclepore filters for counting bacteria by fluorescence microscopy. *Appl. Environ. Microbiol*.**33**, 1225–8

124. Lichtman, J. W., and Conchello, J.A. (2005) Fluorescence microscopy. *Nat. Methods*. **2**, 910–919